

Strain-encoded magnetic resonance: a method for the assessment of myocardial deformation

Grigorios Korosoglou^{1*}, Sorin Giusca¹, Nina P. Hofmann¹, Amit R. Patel², Tomas Lapinskas³, Burkert Pieske^{4,5,6}, Henning Steen⁷, Hugo A. Katus^{8,9} and Sebastian Kelle^{4,5,6}

¹Departments of Cardiology, Vascular Medicine and Pneumology, GRN Hospital Weinheim, Weinheim, Germany; ²Department of Medicine, University of Chicago, Chicago, IL, USA; ³Department of Cardiology, Medical Academy, Lithuanian University of Health Sciences, Kaunas, Lithuania; ⁴Department of Internal Medicine, Cardiology German Heart Center Berlin, Berlin, Germany; ⁵DZHK (German Centre for Cardiovascular Research), Partner Site Berlin, Berlin, Germany; ⁶Department of Internal Medicine/Cardiology, Charité Campus Virchow Clinic, Berlin, Germany; ⁷Department of Cardiology, Marien Hospital Hamburg, Hamburg, Germany; ⁸Departments of Cardiology, Angiology and Pneumology, Heidelberg University, Heidelberg, Germany; ⁹DZHK (German Centre for Cardiovascular Research), Partner Site Heidelberg/Mannheim, Mannheim, Germany

Abstract

This study aims to assess the usefulness of strain-encoded magnetic resonance (SENC) for the quantification of myocardial deformation ('strain') in healthy volunteers and for the diagnostic workup of patients with different cardiovascular pathologies. SENC was initially described in the year 2001. Since then, the SENC sequence has undergone several technical developments, aiming at the detection of strain during single-heartbeat acquisitions (fast-SENC). Experimental and clinical studies that used SENC and fast-SENC or compared SENC with conventional cine or tagged magnetic resonance in phantoms, animals, healthy volunteers, or patients were systematically searched for in PubMed. Using 'strain-encoded magnetic resonance and SENC' as keywords, three phantom and three animal studies were identified, along with 27 further clinical studies, involving 185 healthy subjects and 904 patients. SENC (i) enabled reproducible assessment of myocardial deformation *in vitro*, in animals and in healthy volunteers, (ii) showed high reproducibility and substantially lower time spent compared with conventional tagging, (iii) exhibited incremental value to standard cine imaging for the detection of inducible ischaemia and for the risk stratification of patients with ischaemic heart disease, and (iv) enabled the diagnostic classification of patients with transplant vasculopathy, cardiomyopathies, pulmonary hypertension, and diabetic heart disease. SENC has the potential to detect a wide range of myocardial diseases early, accurately, and without the need of contrast agent injection, possibly enabling the initiation of specific cardiac therapies during earlier disease stages. Its one-heartbeat acquisition mode during free breathing results in shorter cardiovascular magnetic resonance protocols, making its implementation in the clinical realm promising.

Keywords Cardiac magnetic resonance; Strain-encoded MR; SENC; Tagged CMR; Myocardial ischaemia; Viability; Late gadolinium enhancement; Non-ischaemic cardiomyopathy; Heart failure; Diabetic heart disease; Diastolic function; Right ventricle; Cardiotoxicity

Received: 2 November 2018; Accepted: 28 March 2019

*Correspondence to: Grigorios Korosoglou, Department of Cardiology and Vascular Medicine, GRN Academic Teaching Hospital Weinheim, Roentgenstrasse 1, D-69469 Weinheim, Germany. Tel: +49 6201 89 2142; Fax: +49 6201 89 2507. Email: grigorios.korosoglou@grn.de

Introduction

Changes of the myocardium in shape and dimensions during the cardiac cycle can be characterized by the assessment of myocardial 'strain', which is a measure of deformation, i.e. regional shortening, thickening, and lengthening of the myocardium. The term strain originates from the field of physics, where it used to describe the deformation of a small cube during a very short time interval along the three dimensions

in space. For the heart, an internal coordinate system aligned with the three cardiac axes is used: longitudinal, circumferential, and radial, to measure myocardial strain (i.e. shortening and elongation) in these three predefined directions throughout the cardiac cycle.

Strain-encoded magnetic resonance (MR) (SENC) is an advanced tagging technique, which provides both colour-coded visual and quantitative assessment of myocardial strain. SENC is an evolution of the myocardial tagging pulse

sequence.^{1,2} It differs in that the tags are applied as a series of planes in the through-plane direction rather than as a series of lines in the in-plane direction. As the myocardium contracts, the planes in the through-plane direction compress together. This causes a shift in the location of the peak spectrum in k space. The rate of this shift can be used to determine myocardial strain. Image reconstruction is then tuned to the high or the low frequency peak to create an image that represents systolic or diastolic strain, respectively, as demonstrated in Supporting Information, *Figure S1*. SENC was introduced by Osman *et al.*¹ and was subsequently modified by Pan *et al.*, who implemented reduced field of view using selective excitation, spiral data acquisition, and interleaved low and high tuning with the original SENC sequence, allowing the assessment of myocardial strain during real-time acquisitions.³ This single-heartbeat imaging sequence was called 'fast-SENC'. Typical parameters on the spatial and temporal resolution of the SENC and the fast-SENC sequence and a comparison with standard cine, tagged MR, and late gadolinium enhancement (LGE) sequences are provided in Supporting Information, *Table S1*.

Myocardial strain using SENC can be assessed using the software provided by Myocardial Solutions Inc., Morrisville, NC, USA, which is commercially available. The software automatically delineates the myocardium, providing colour-coded illustration of contracting myocardial tissue throughout the cardiac cycle. The observer can interact by adjusting the delineation of the myocardium. In addition, the observer can manually set a region of interest to quantify myocardial strain in a specific region of the myocardium. Increased heart rate and motion artefacts need to be considered during image acquisition with the SENC sequence, which is currently available as a product with Philips scanners and as a patch with other vendors. Because the typical temporal resolution is lower with real-time acquisitions (see Supporting Information, *Table S1*), this may pose a limitation with strain assessment during dobutamine stress, which can be better assessed using the conventional SENC sequence. In addition, exact alignment of the imaging planes is necessary if a comparison is intended with cine or tagging acquisitions. In this regard, movement of the patient between the different acquisitions may hamper comparison of the acquired data. Motion and breathing artefacts are of course a problem with all cardiovascular magnetic resonance (CMR) sequences, including cine, tagging, and SENC. With fast-SENC, such motion and breathing artefacts are less pronounced due to fast acquisition, which can be performed during free breathing.

In this article, we give an overview of studies where SENC and fast-SENC were used to quantify deformation *in vitro*, in animal models and in humans. Such clinical applications with SENC and fast-SENC may contribute to earlier diagnosis of

coronary artery and myocardial diseases, enabling initiation of treatment in earlier disease stages with the potential to improve long-term outcomes.

The summary of such clinical applications will motivate the reader to consider future applications of SENC in the field of cardiovascular medicine.

Assessment of deformation *in vitro*

In vitro studies previously demonstrated that SENC can be used to obtain mechanical tissue properties.^{4–6} In these *in vitro* experiments, tissue phantoms with different density and stiffness and *ex vivo* human tumour specimens were systematically examined. In contrast to conventional MR techniques such as T_1 -weighted imaging,⁵ which were only able to distinguish stiffer tumours from normal tissue, SENC enabled precise measures of strain, which was inversely related to tumour stiffness.^{4–6} Thus, with soft masses, SENC exhibited strain values of between 35% and 50%, whereas with harder masses, strain values were between 0% and 20%. In this way, SENC enabled light to be shed on mechanical tissue properties by estimating strain in breast tumours, which allowed the detection of both stiffer and softer tumour lesions compared with their background tissue. Due to the high spatial resolution of the SENC sequence in this study (in-plane resolution of $1 \times 1 \text{ mm}^2$), detailed delineation of the tumours was possible with high image quality.⁴

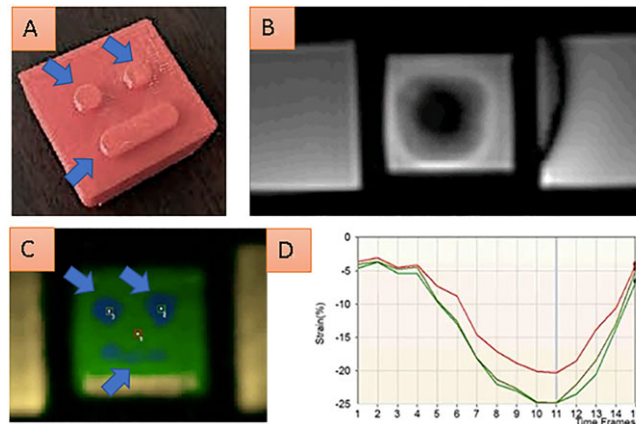
The ability of SENC to delineate non-uniform compression of an *in vitro* gel phantom can be appreciated in *Figure 1*. Using SENC image details (blue arrows in A and in C) can be precisely detected during non-flat compression of the gel phantom. Such image details are completely missed by conventional cine balanced steady-state free precession sequences.

Myocardial strain in animals studies

Several experimental studies have investigated the ability of strain quantification to serially assess myocardial function in animal models. Controlled conditions during animal experiments give the opportunity to judge the effectiveness of surgical and pharmacological interventions in models of various cardiac diseases and to correlate functional measurements to histopathologic studies.⁷

Using SENC, Ibrahim *et al.* measured regional myocardial strain using SENC in five pigs, including two that underwent a closed-chest procedure to induce myocardial infarction.⁸ In this study, non-contracting myocardial regions due to infarction exhibited good agreement with corresponding infarcted myocardial tissue by LGE imaging. In addition, the ability of SENC to detect changes in regional contraction

Figure 1 A gel phantom, which is non-flat compressed during our *in vitro* experiment is shown in A. SENC can precisely delineate non-uniform compression of the phantom, which enables detection of image details (blue arrows in A and in C). Image details are completely missed by the conventional cine fiesta sequence (B). Quantification analysis of three points over the time of non-flat compression is shown in D.



was recently demonstrated in an experimental porcine model.^{9,10} Thus, in myocardial areas where an extracellular matrix patch derived from porcine small intestine submucosa was implanted, regional myocardial contraction increased due to generation of functional myocardial tissue in these areas, and this could be depicted by SENC. These approaches are promising for the assessment of functional properties of the myocardium before and after the implantation of tissue-engineering devices for the treatment of advanced heart failure.

In *Figure 2*, the midventricular short axis view of a porcine heart in the setting of experimental myocardial infarction after closure of its circumflex coronary artery can be appreciated with cine imaging in A and B, LGE in C, and conventional SENC imaging in D and E, including quantitative analysis in F. SENC demonstrates deteriorated regional strain in the lateral left ventricular (LV) wall, which corresponds to areas of infarcted myocardium shown by LGE.

SENC in the healthy human heart at baseline and during inotropic stimulation

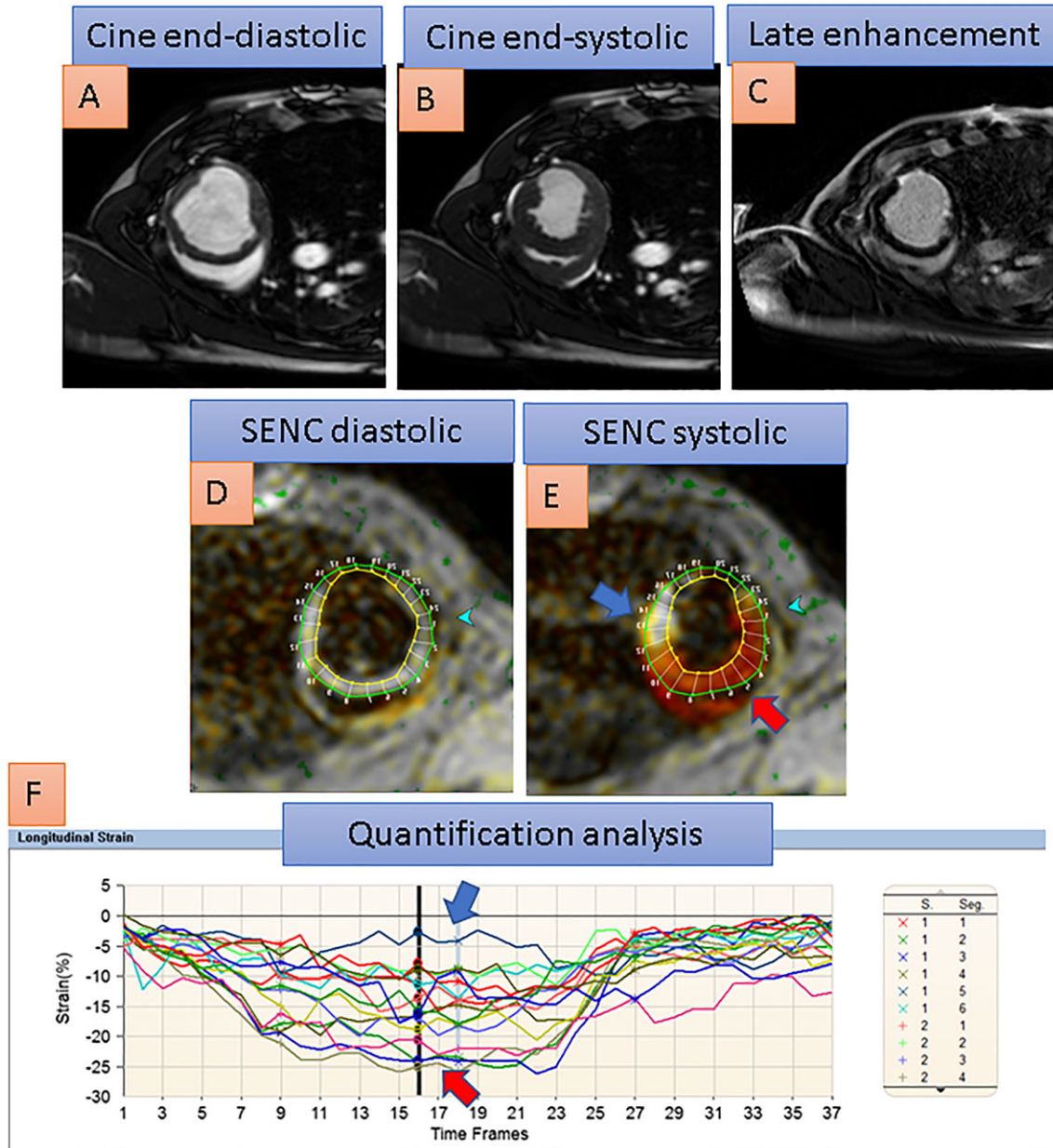
Almost two decades ago, tagged MR studies conducted in healthy subjects demonstrated that myocardial strain is non-uniform within the human heart, varying between different regions of the myocardium. Possible explanations for this functional heterogeneity are morphologic differences in LV architecture, which are attributed to variable transmural fibre orientation at a microscopic level.¹¹

Garot *et al.* used SENC to assess myocardial strain in five healthy volunteers.¹² Strain values obtained by SENC were

strongly related to those obtained by tagged MR. Importantly, the time spent for complete analysis was ~6–8 h for 3D tagged MR, which was substantially higher than the ~35 s required for segmentation of the LV and calculation of myocardial strain with SENC. Ibrahim *et al.* also used SENC to measure circumferential and longitudinal strain in 10 healthy volunteers. In this study, a real-time SENC imaging pulse sequence was used, which considers through-plane motion of the heart. This pulse sequence was tested in an experimental model of myocardial infarction in pigs in the same study, and the resultant SENC images were compared with LGE, showing good agreement for the identification of infarcted myocardium.⁸ The utility of the real-time imaging SENC technique to assess regional myocardial strain was then applied in 12 volunteers, using tagged MR as the standard reference technique.¹³ Experimental validation of myocardial tagging has been previously performed using sonomicrometry, which was performed in dogs after implantation of CMR visible sonomicrometers into the myocardium.¹⁴ Peak systolic strain (maximal strain during systole) and early diastolic strain rate values (diastolic strain rate during the early diastole) acquired by SENC were closely related to tagged MR. Furthermore, SENC showed high sensitivity for the detection of differences between subendocardial and epicardial regions for systolic and for diastolic function. Breath-hold time was much shorter with SENC than with conventional tagging, whereas quantitative analysis was less time consuming.¹³

SENC was also used for the evaluation of circumferential and longitudinal strain in 75 healthy volunteers (35 women and 40 men, mean age 44 ± 12 years, range between 22 and 69 years) by a clinical 1.5 T system.¹⁵ All subjects underwent extensive clinical and biochemical tests, including glucose tolerance, liver enzymes, differential blood

Figure 2 The midventricular short axis view of a porcine heart with akinesia of the lateral left ventricular wall after infarction due to closure of its circumflex coronary artery can be appreciated with cine images in A and B. With conventional SENC images, red colour corresponds to normal contracting myocardium in the septal wall, faded orange and yellowish colour corresponds to reduced strain in peri-infarct areas, and white colour corresponds to severely reduced or absent myocardial contraction in the infarcted lateral wall. Late gadolinium enhancement (in C) exhibits 75% transmural infarction of the lateral wall, which corresponds to severely reduced strain, coded white in the lateral wall (blue arrow) compared with normal strain, coded red in the septal wall (red arrow), with the systolic SENC image in E. Quantification analysis in F reveals severely reduced systolic strain in the lateral wall segments (blue arrow in F) compared with normal strain in septal wall segments (red arrow in F).



count, renal function, cardiac troponins, and NT-proBNP before inclusion in the study. Dobutamine stress MR was conducted in all subjects. The study showed that peak systolic strain values exhibited close correlation and close limits of agreement with tagged MR. Regional heterogeneity was observed for longitudinal strain values by SENC, with

myocardial strain values varying in different regions of the myocardium. The evaluation of the diastolic LV function was also feasible with SENC, which, in line with previous studies, demonstrated markedly diminished circumferential diastolic strain rate in older patients vs. younger subjects (75.9 ± 24 ECC/s vs. 122.3 ± 36 ECC/s, $P < 0.001$), possibly

due to increasing myocardial fibrosis and stiffness in older subjects.¹⁵ Inter-observer variability was excellent for SENC and superior to that provided by tagged MR by z-statistics ($r = 0.87$ for SENC vs. $r = 0.81$ for tagged MR; $P < 0.05$).¹⁵ The strain values measured in this study are similar to those measured by earlier implementations of the SENC sequence in previous studies.^{8,13} Generally, SENC may be superior for the assessment of diastolic function as, in contrast to conventional tagging, SENC does not suffer from loss of contrast-to-noise ratio of the MR tags during the diastole. From a clinical point of view, this appears very important, because diastolic dysfunction is increasingly being appreciated as a major cause of heart failure.¹⁶

In another study, Hamdan *et al.* demonstrated the ability of SENC to assess regional LV function and timing of contraction in a clinical 3 T scanner.¹⁷ In this study, inter-study reproducibility was tested, exhibiting very high interclass correlation coefficients of 0.96 to 0.98 for circumferential and longitudinal strain, respectively. It should be noted that SENC provides higher temporal resolution of 14–25 ms, which allows evaluation of the time sequence of myocardial deformation with higher accuracy compared with conventional tagging, which has a typical temporal resolution of ~30–40 ms.

Youssef *et al.* studied systolic circumferential strain of the right ventricle in 21 healthy subjects who underwent 3.0 T cardiac MR. SENC depicted increasing circumferential strain from the base to the apex of the right ventricular (RV) free wall and demonstrated excellent inter-observer and intra-observer variabilities, as indicated by the interclass correlation coefficients of $r = 0.82/0.81$, $0.80/0.79$, and $0.94/0.81$ for the basal, mid, and apical RV regions, respectively.¹⁸ In addition, longitudinal and circumferential strain of the right ventricle was assessed in another 11 healthy subjects using single-heartbeat fast-SENC.¹⁹ In this study, a high correlation was observed between conventional SENC and single-heartbeat fast-SENC acquisitions, whereas the previously reported heterogeneous pattern of RV circumferential shortening was confirmed, exhibiting higher absolute values in basal and lower absolute values in midventricular and apical RV regions.

The ability of SENC to evaluate myocardial strain of the left ventricle in healthy subjects during inotropic stimulation with dobutamine was demonstrated in two further studies, involving 17 and 18 healthy subjects, respectively.^{20,21} In both studies, quantitative analysis of SENC images was conducted, demonstrating that systolic strain remains constant during inotropic stimulation. Strain rate (i.e. the rate of myocardial deformation in time, expressed in 1 s^{-1}), on the other hand, increased stepwise during lower stages of inotropic stimulation, reaching ~2-fold values compared with baseline.

An overview of all studies investigating myocardial strain using SENC in the normal heart can be found in *Table 1*.

High accuracy for the detection of coronary artery disease without the need for contrast agent administration

The role of CMR is clinically well established for the diagnostic classification²² and risk stratification²³ of patients with ischaemic heart disease. Thus, referral for a CMR examination of ~50% of patients within the European cardiovascular magnetic resonance registry (Euro-CMR) is related to the diagnostic workup for ischaemic heart disease.²⁴ The cost-effectiveness of such a 'non-invasive' CMR approach vs. an invasive diagnostic strategy using X-ray angiography and fractional flow reserve (FFR) measures in patients with low to intermediate disease prevalence was also recently demonstrated.²⁵

However, the detection of inducible ischaemia by adenosine or dobutamine CMR is currently based on the visual assessment of perfusion defects or wall motion abnormalities during stress, which is both subjective and depends on the experience of the readers. In addition, with wall motion, the human eye focuses on radial motion of the myocardium in cine images, which is less sensitive for the detection of myocardial dysfunction, compared with circumferential and longitudinal contraction.^{26–29}

Several clinical studies investigated the ability of SENC for the detection of myocardial ischaemia during pharmacologic stress with high-dose dobutamine and atropine stimulation.^{20,21,30,31} In one of these studies, a head-to-head comparison was performed between conventional cine, tagged MR, and SENC, using invasive coronary angiography as the reference standard (lumen narrowing >50%).³¹ Analysis was conducted by visual criteria in 65 patients with suspected or known coronary artery disease (CAD). SENC contributed to improved sensitivity compared with tagged MR and cine imaging for CAD detection (sensitivity of 89% for SENC vs. 81% by tagging and 70% by cine imaging, $P < 0.05$ for tagging and $P < 0.01$ for SENC), whereas specificity and overall accuracy were similar between the three techniques (94% for SENC vs. 96% for tagging and 95% cine for specificity and 92% for SENC vs. 91% for tagging and 87% for cine for accuracy, $P =$ not significant for all).

In a further step, SENC was compared with cine imaging for the detection of myocardial ischaemia during dobutamine stress CMR in 101 patients with suspected or known CAD.³⁰ SENC detected abnormal strain response in eight patients, who were completely missed by conventional cine imaging, exhibiting higher sensitivity and overall accuracy for the detection of CAD [sensitivity of 85% by SENC vs. 70% by cine ($P < 0.01$) and accuracy of 91% by SENC vs. 87% by cine ($P < .05$)]. Quantitative analysis was performed in this study by calculating the following ratios on a segmental basis:

Table 1 Summary of the studies investigating normal values for SENC in the right and left ventricle of the heart in healthy subjects

First author, journal, and year of publication	Number of volunteers	Region of interest	Comparison with tagged MR	Single-heartbeat acquisitions	Mean longitudinal strain values	Mean circumferential strain values
Garot <i>et al.</i> , <i>Radiology</i> , 2004	5	Left ventricle	Yes	No	10.6 ± 0.5 ^b	NA
Ibrahim <i>et al.</i> , <i>JMRI</i> , 2007	10	Left ventricle	Yes	No	17.8 ± 1.3	21.0 ± 1.2
Korosoglou <i>et al.</i> , <i>JMRI</i> , 2008	12	Left ventricle	Yes	Yes	NA	21.7 ± 2.7
Neizel <i>et al.</i> , <i>JMRI</i> , 2009	75	Left ventricle	Yes	No	19.5 ± 2.9 to 24.3 ± 3.2 ^a	19.5 ± 3.2 to 23.7 ± 3.1 ^a
Hamdan <i>et al.</i> , <i>JMRI</i> , 2009	16	Left ventricle	No	No	16.4 ± 1.6 to 22.3 ± 1.8 ^a	14.0% ± 1.8% to 22.0 ± 3.0 ^a
Youssef <i>et al.</i> , <i>JCMR</i> , 2008	21	Right ventricle	No	No	NA	18.7 ± 4.3
Shehata <i>et al.</i> , <i>MRM</i> , 2010	11	Right ventricle	Yes	Yes	21.8 ± 2.0 for the RV base ^c	21.8 ± 1.9 for the RV base ^c
Korosoglou <i>et al.</i> , <i>Circulation</i> , 2009	17	Left ventricle ^d	No	No	NA	21.5 ± 2.2
Korosoglou <i>et al.</i> , <i>JACC CVI</i> , 2010	18	Left ventricle ^d	No	No	19.2 ± 3.4	21.8 ± 3.8

MR, magnetic resonance; NA, not applicable; RV, right ventricular.

Strain values are given as absolute values.

^aRegional heterogeneity was observed with different values among different segments. The value for the segments with the lowest and the highest strain values is provided, respectively.

^bLongitudinal SENC values in this study are lower than those measured in all other subsequent studies, which may be attributed to an older implementation of the SENC pulse sequence at that time point.

^cIncreasing values of absolute strain were observed from the base to the apex of the right ventricle.

^dStudies performed at baseline and during inotropic stimulation with dobutamine.

$$S_{\text{Reserve}} = \frac{S_{\text{peak-stress}}}{S_{\text{baseline}}} \quad \& \quad SR_{\text{Reserve}} = \frac{SR_{\text{peak-stress}}}{SR_{\text{baseline}}}$$

S indicating strain and SR indicating strain rate

Strain rate reserve was closely related to coronary lumen narrowing ($r^2 = 0.56$, $P < 0.001$), and a cut-off value of strain rate reserve = 1.64 exhibited high accuracy for the detection of >50% stenosis (area under the curve, 0.96; standard error, 0.01; 95% confidence interval, 0.94 to 0.98; $P < 0.001$).

In another study, quantitative analysis of SENC images was used to study myocardial strain and strain rate response during different stages of inotropic stimulation in healthy volunteers ($n = 18$) and in patients with suspected or known CAD ($n = 80$). Circumferential myocardial strain remained constant during stress in non-ischaeamic segments (-20 ± 4.2 at baseline vs. -22 ± 3.5 during intermediate stress vs. -20 ± 3.7 during peak stress), whereas it decreased stepwise in segments supplied by obstructed coronary arteries (-19 ± 4.2 at baseline vs. -16 ± 6.2 during intermediate stress vs. -13 ± 6.4 during peak stress).²¹ Strain rate, on the other hand, increased stepwise during stress in non-ischaeamic myocardial segments (-1.3 ± 0.4

during baseline vs. -2.1 ± 0.7 during intermediate stress vs. -3.8 ± 1.2 at peak stress), whereas it remained constant in ischaemic segments (-1.5 ± 0.4 during baseline vs. -1.7 ± 0.7 during intermediate stress vs. -1.6 ± 0.9 during peak stress). This different circumferential strain and strain rate responses allowed differentiation between patients with and without obstructive CAD already during intermediate stages of inotropic stimulation at 20 $\mu\text{g}/\text{kg}/\text{min}$, which can increase patient safety and reduce time spent with diagnostic imaging procedures. In addition, the cost-effectiveness of SENC for the detection of CAD compared with SPECT, providing monetary savings for patients and resource benefits for hospitals, was recently demonstrated.³²

Apart from the diagnostic classification of patients with CAD, the assessment of prognosis was a central clinical goal with dynamic SENC studies. Thus, in a relatively large cohort of patients ($n = 320$) who underwent high-dose dobutamine stress CMR, SENC allowed the differentiation of patients with normal findings and a low rate of cardiac events from those with abnormal findings and increased rates of subsequent hard cardiac events (i.e. revascularization procedures).²⁰ Using the Cox proportional hazards models, inducible wall motion abnormality (WMA) by cine (new or worsening

WMA of ≥ 1 grade during stress) offered incremental information for the assessment of hard cardiac events compared with clinical variables ($\chi^2 = 13.0$ for clinical vs. $\chi^2 = 39.3$ by adding inducible WMA, $P < 0.001$). By adding SENC (strain reduction of ≥ 1 grade during stress with colour-coded images), prediction of outcome further significantly improved compared with cine imaging ($\chi^2 = 50.7$, $P < 0.001$).

Table 2 provides an overview of studies investigating myocardial strain during pharmacologic stress. In Figure 3, inducible ischaemia of the inferior wall during high-dose dobutamine stress was missed by conventional cine (A and B) and by tagged MR (C and D) but can be detected by conventional SENC images (E and F, blue arrow in F) in a patient with significant lumen narrowing in the right coronary artery.

Non-inferiority for the detection of myocardial infarction and viability compared with late gadolinium enhancement

In patients with acute myocardial infarction, previous CMR trials demonstrated that the assessment of infarct size and transmural, as well as the presence of microvascular obstruction, can predict recovery of systolic function, adverse remodelling, and clinical outcomes (reviewed in Reinstadler *et al.*³³). In patients with chronic infarction on the other hand, the identification of viable myocardium is an important clinical goal, because the revascularization of hibernating myocardium is associated with improvement in LV function and favourable outcome.³⁴ In this setting, infarct transmural by LGE is well established.²² However, with LGE, a grey zone exists for segments with infarct transmural of between 25% and 75%, as such segments show a variable range for functional recovery after revascularization of between 10% and 64%.^{35–37} In addition, even with clinically well-established LGE sequences, early image acquisition after contrast agent administration can lead to substantial overestimation of infarct size, especially in non-transmural infarctions, where LGE can be present in areas of salvaged myocardium.³⁸

Several studies investigated the value of SENC for the assessment of myocardial viability. In this regard, a good

correlation was observed between SENC and tagged MR for the evaluation of myocardial strain, whereas quantitative analysis by SENC was substantially less time consuming.¹² Interestingly, the extent of dysfunctional myocardium by SENC was greater than the areas of LGE, underscoring the fact that reduced function is present not only in areas of infarcted myocardium but also in adjacent tissue, which agrees with previous observations.³⁹

Two other studies used SENC to examine circumferential and longitudinal myocardial strain in 50 and 29 patients, respectively, with chronic infarction and using LGE as the reference standard technique for the evaluation of myocardial viability.^{40,41} A cut-off value of -15% for circumferential strain using SENC was selected by the authors, which aided the differentiation between non-transmural and transmural myocardial infarction, providing sensitivity of 100% and specificity of 86%.⁴⁰ The ability of SENC to differentiate between subendocardial and transmural myocardial infarction was confirmed in another study using single-heartbeat fast-SENC acquisitions in 19 patients with chronic ischaemic heart disease.⁴²

In the setting of acute myocardial infarction, SENC was also used for the differentiation between viable and irreversibly injured myocardial tissue with high accuracy.⁴³ Thus, in 38 patients with first-time acute myocardial infarction, a cut-off value of -10% for peak circumferential strain differentiated non-transmural from transmural infarction with very high sensitivity of 97% and specificity of 94%. Strain analysis by SENC closely correlated to tagged MR, which was also performed in this study, demonstrating narrow limits of agreement between the two techniques. Taking it a step further, the ability of systolic and diastolic deformation indexes acquired by SENC was examined for the prediction of functional recovery in 26 patients with reperfused myocardial infarction by Neizel *et al.*⁴⁴ In this study, circumferential strain decreased with increasing infarct transmural by LGE (-13 ± 6 with infarct transmural 0–25% vs. -11 ± 8 with infarct transmural 26–50% vs. -8 ± 7 with infarct transmural 51–75% vs. -4 ± 6 with infarct transmural 76–100%). Regional early diastolic strain rate exhibited higher accuracy than systolic strain indexes and similar accuracy to that provided by the reference standard LGE for the prediction of contractile myocardial recovery at 6 months of follow-up. Thus, the assessment of regional diastolic function may serve as a useful

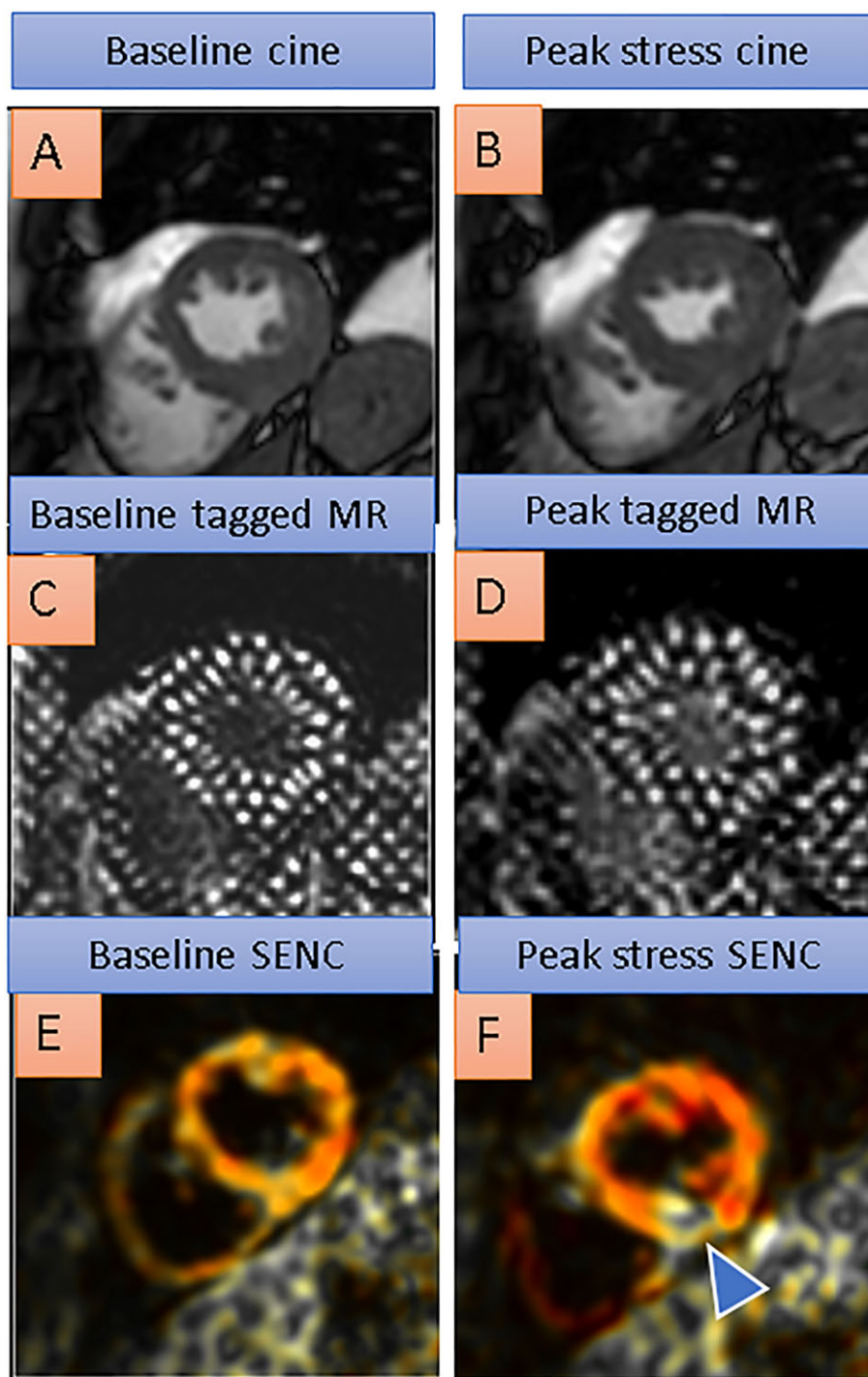
Table 2 Summary of the studies investigating the ability of SENC for the detection of myocardial ischaemia during stress

First author, journal, and year of publication	Number of patients	Visual analysis	Quantitative analysis	Comparison with tagged MR	Sensitivity (%)	Specificity (%)
Korosoglou <i>et al.</i> , <i>JMRI</i> , 2009	65	Yes	No	Yes	89	94
Korosoglou <i>et al.</i> , <i>Circulation CVI</i> , 2009	101	Yes	Yes	No	85	94
Korosoglou <i>et al.</i> , <i>JACC CVI</i> , 2010	80	Yes	Yes	No	76 ^a	88 ^a
Korosoglou <i>et al.</i> , <i>JACC</i> , 2011	320	Yes	Yes	No	96	88

MR, magnetic resonance.

^aSensitivity and specificity during intermediate stages (20 $\mu\text{g}/\text{kg}/\text{min}$) of inotropic stimulation.

Figure 3 Baseline cine, tagged magnetic resonance (MR), and SENC images on the left compared with peak dobutamine stress images on the right side. Inducible ischaemia of the inferior wall during high-dose dobutamine stress is missed by conventional cine (A and B) and by tagged MR (C and D) but can be detected by conventional SENC images (E and F, blue arrowhead in F depicting reduced strain response during dobutamine stress in the inferior left ventricular wall, coded yellowish/white compared with normal strain in the corresponding anterior wall, coded red) in a patient with a right coronary artery stenosis.



parameter for the assessment of myocardial viability after acute myocardial infarction, especially in patients with contraindications to contrast agent administration. It should be

noted, however, that so far only this study demonstrated the ability of SENC to predict contractile myocardial recovery in the setting of acute infarction, whereas data are still lacking

in the setting of non-reperfused acute infarction and with chronic infarction.

An overview of the studies investigating the assessment of myocardial viability with SENC is found in *Table 3*. *Figure 4* shows single-heartbeat fast-SENC images of a 59-year-old patient with ischaemic cardiomyopathy (ejection fraction of ~30%) due to old anterior wall infarction. Systolic SENC images show reduced strain in the anterior and septal wall (B and E), which corresponds to areas of transmurally infarcted myocardium in C and in F.

Early detection of vasculopathy in heart transplant recipients

Cardiac allograft vasculopathy (CAV) is a particular type of atherosclerosis, which progressively causes diffuse and concentric thickening of coronary vessels, compromising perfusion in heart transplant recipients and ultimately leading to congestive heart failure and death.^{45–47} Currently, routine coronary angiography is widely used to detect CAV in cardiac transplant recipients, independently of the presence of clinical symptoms. However, assessment of lumen narrowing on angiograms can underestimate concentric thickening of the coronary artery wall and also provides little information on microvascular integrity of the myocardium,⁴⁸ thus yielding low sensitivity for the detection of CAV.

Previous studies demonstrated that CMR can detect early stages of CAV by the International Society for Heart and Lung Transplantation criteria, identifying underlying myocardial perfusion abnormalities⁴⁹ or myocardial fibrosis by LGE⁵⁰ in transplant recipients with preserved LV function. In addition, the utility of SENC for the quantification of systolic strain and diastolic strain rate in heart transplant recipients has been demonstrated.⁵¹ In this regard, reduced myocardial perfusion reserve, measured by dividing the contrast agent upslope

during pharmacologic hyperaemia with adenosine through the upslope at baseline, was closely related to impaired diastolic strain rate, aiding the early detection of subclinical CAV. In addition, reduced diastolic strain rate by SENC was closely associated with thickened coronary arterioles and diminished capillary density by histopathology and caused poorer outcomes in heart transplant recipients, compared with patients with normal diastolic strain rate.⁵² Thus, a normal cardiac CMR in terms of diastolic strain rate by SENC and myocardial perfusion reserve may obviate the need for invasive procedures for the next 2–3 years, in the interest of reduced potential nephrotoxicity and increased patient safety.

In *Figure 5*, the images from a heart transplant recipient with normal coronary arteries by angiography and preserved ejection fraction of 55% are shown. Using conventional SENC, reduced systolic strain can be depicted in the basal anterior wall (blue arrow in B), whereas reduced diastolic strain, indicating impaired diastolic LV function, is demonstrated by quantitative analysis in three different myocardial regions in I (mean early diastolic strain rate of ~50 s, normal >80 s). In agreement with these findings, the patient exhibited thickened coronary arterioles and reduced capillary density (G and H) by histologic criteria and was diagnosed with CAV.

Detection of global and regional dysfunction in non-ischaemic cardiomyopathies and inter-study variability

Non-ischaemic cardiomyopathies represent a heterogeneous group of myocardial disorders, which are frequently associated with inappropriate ventricular hypertrophy or dilatation. Among this heterogeneous group of diseases, which are

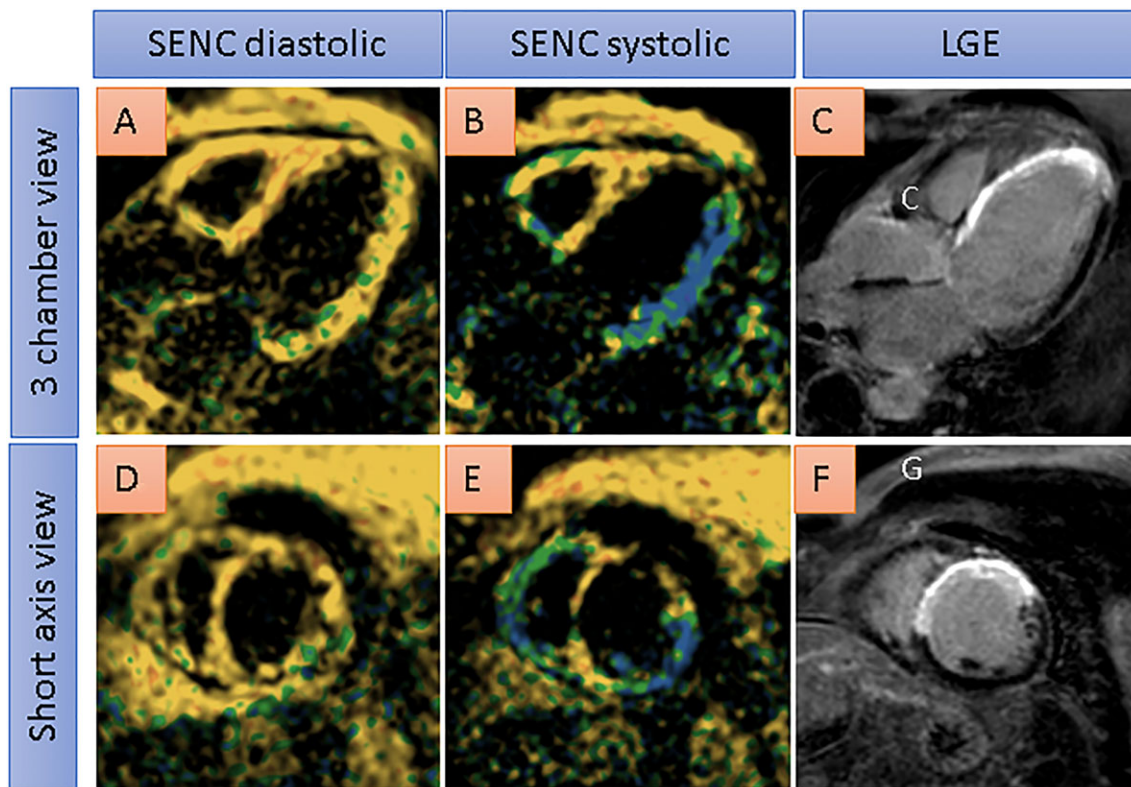
Table 3 Summary of the studies investigating the ability of SENC for the detection of myocardial viability in ischaemic heart disease

First author, journal, and year of publication	Number of patients	Quantitative analysis	Comparison with tagged MR	Comparison with LGE	Functional recovery	Sensitivity (%)	Specificity (%)
				Chronic infarction			
Garot <i>et al.</i> , <i>Radiology</i> , 2004	9	Yes	Yes	Yes	No	NA	NA
Koos <i>et al.</i> , <i>International Journal of Cardiology</i> , 2011	50	Yes	No	Yes	No	100	86
Altiok <i>et al.</i> , <i>European Heart Journal CVI</i> , 2013	29	Yes	No	Yes	No	86	51
Oyama-Manabe <i>et al.</i> , <i>European Radiology</i> , 2011	19	Yes	No	Yes	No	95	47
				Acute infarction			
Neizel <i>et al.</i> , <i>Circulation CVI</i> , 2009	38	Yes	Yes	Yes	No	97	94
Neizel <i>et al.</i> , <i>JACC</i> , 2013	26	Yes	No	Yes	Yes	82 ^a	75 ^a

LGE, late gadolinium enhancement; MR, magnetic resonance; NA, not applicable.

^aCut-off value of <31 s for early diastolic strain rate.

Figure 4 Single-heartbeat fast-SENC images from a 59-year-old patient with ischaemic cardiomyopathy (ejection fraction of ~30%) due to old anterior wall infarction. Systolic SENC images show severely reduced strain in the anterior and septal wall (coded yellow in B and E), which corresponds to areas of transmurally infarcted myocardium by late gadolinium enhancement (LGE) imaging in C and F. With conventional single-heartbeat fast-SENC images, blue colour corresponds to normal contracting myocardium, green colour corresponds to reduced strain, and yellow colour corresponds to severely reduced or absent myocardial contraction.



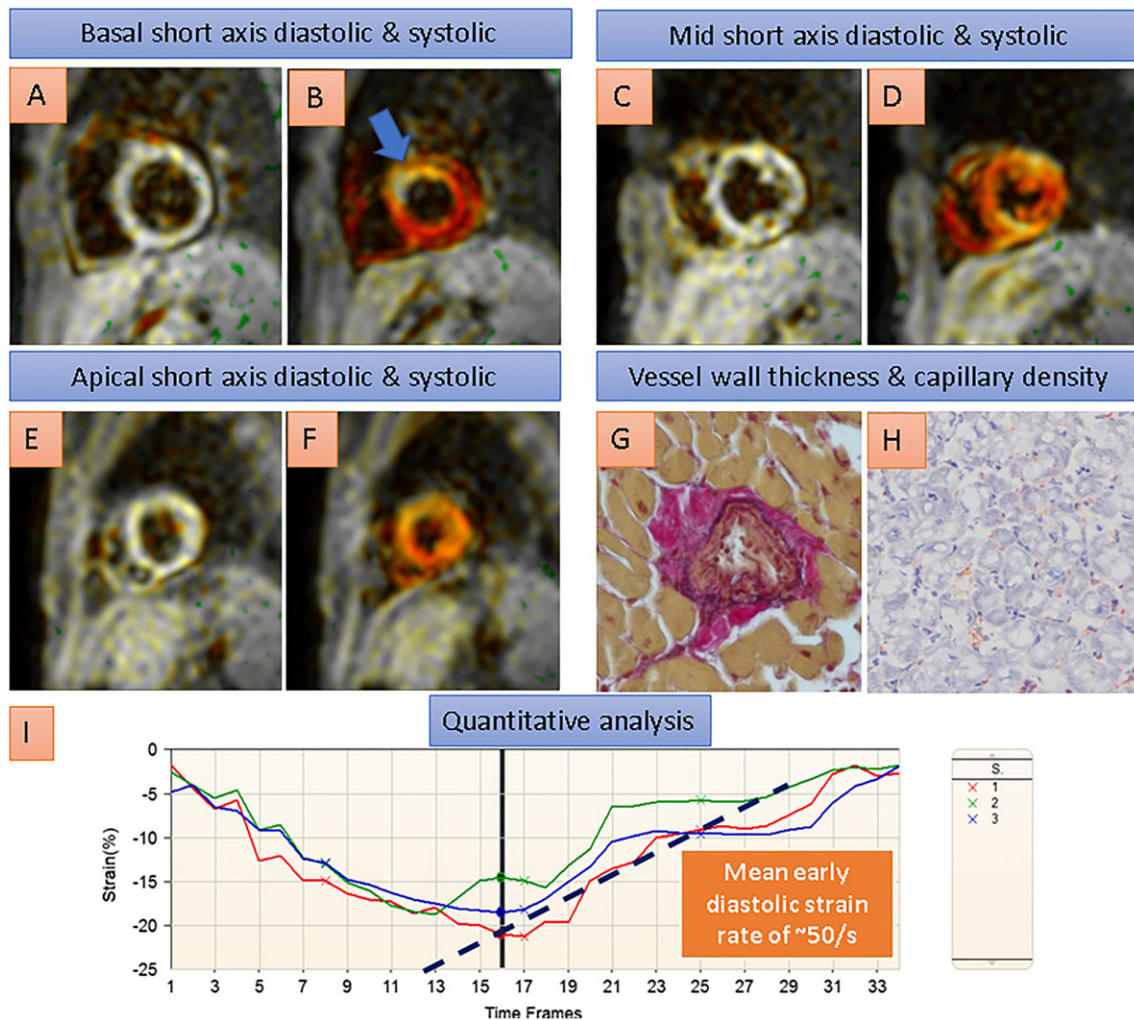
frequently associated with genetic disorders, dilated cardiomyopathy (DCM) and hypertrophic cardiomyopathy (HCM) are the most common, accounting for a substantial proportion of cardiac mortality.⁵³

The versatility of CMR can provide diagnostic workup of patients with DCM, HCM, and cardiac amyloidosis or sarcoidosis, enabling the reproducible assessment of LV function, mass, and fibrosis by LGE, which has been identified as an independent prognostic marker in such patients.^{54–56} Using fast-SENC, differences in both systolic strain and early diastolic strain rates could be identified in patients with ischaemic and non-ischaemic cardiomyopathies, compared with control subjects.¹³ This finding was confirmed in a very recent study by Giusca *et al.*,⁵⁷ who examined 11 healthy individuals and 7 patients with heart failure using fast-SENC acquisitions for the evaluation of global longitudinal strain (GLS) and global circumferential strain (GCS) and LV ejection fraction. The CMR scans were repeated after a median of 63 days, and SENC images were analysed by two experienced observers. As expected, patients with heart failure exhibited lower GLS and GCS than healthy individuals. In addition, test–retest analysis demonstrated excellent intraclass

coefficients for GLS and GCS. GLS and GCS showed overall narrower limits of agreement for both intra-observer and inter-observer variability (–0.6 to 0.5 for intra-observer and –1.3 to 0.96 for inter-observer agreement for GLS and –1.1 to 1.2 for intra-observer and –1.7 to 1.3 for inter-observer agreement for GCS) compared with LV ejection fraction, which exhibited larger limits of agreement (–14.4 to 10.1). An overview of studies providing inter-observer and intra-observer as well as inter-study agreements with visual and quantitative SENC studies is given in Supporting Information, *Table S2*.

With HCM, on the other hand, longitudinal and circumferential strain was measured using SENC in 22 patients with HCM and in 24 age-matched control subjects, who underwent CMR inducing LGE imaging. Hereby, GLS was reduced in patients with HCM compared with control subjects. In addition, regional heterogeneity of circumferential strain was predictive of extensive LGE ($\geq 15\%$ of the LV mass) in patients with HCM with high sensitivity of 83% and specificity of 94%, whereas longitudinal strain was less helpful for the identification of patients with extensive fibrosis.⁵⁸

Figure 5 A heart transplant recipient with normal coronary arteries by angiography and normal ejection fraction of 55% by cardiovascular magnetic resonance. In this patient, conventional SENC acquisitions depicted reduced systolic strain in the basal anterior wall (blue arrow in B, coded yellowish/white compared with normal strain, e.g. in the inferior wall, coded red), and reduced diastolic strain rates, indicating impaired diastolic left ventricular function, were demonstrated by quantitative analysis of the strain curves in I. Endomyocardial biopsy showed thickened coronary arterioles and reduced capillary density (G and H) by histologic criteria, consistent with transplant microvasculopathy.



For cardiac sarcoidosis, limited data exist on the usefulness of echocardiographic derived strain for the detection of myocardial fibrosis by CMR.⁵⁹ In a recent case report, longitudinal strain measured by SENC was proposed as a very sensitive marker compared with circumferential strain and LGE for the detection of regional myocardial dysfunction and for the judgment of the effectiveness of immunosuppressive therapy in a patient with cardiac sarcoidosis.⁶⁰

An overview of studies investigating the role of SENC in patients with non-ischaemic cardiomyopathies is provided in Table 4.

Single-heartbeat fast-SENC acquisitions of a patient with DCM (A–E) and another patient with HCM (F–I) are provided in Figure 6. Images of a patient with atrial fibrillation and

DCM are shown in A–E. Despite atrial fibrillation, high image quality can be achieved, showing reduced strain using fast-SENC in A and C. Ejection fraction is ~20% with cine images in B (mid short axis) and D (four-chamber view). The electrocardiogram demonstrates atrial fibrillation (E). Images of a patient with HCM are shown in F–I. Severe LV hypertrophy with reduced myocardial strain, especially in the LV septum and in the anterior wall, is revealed by fast-SENC (F and H). Systolic cine images are provided in G and I.

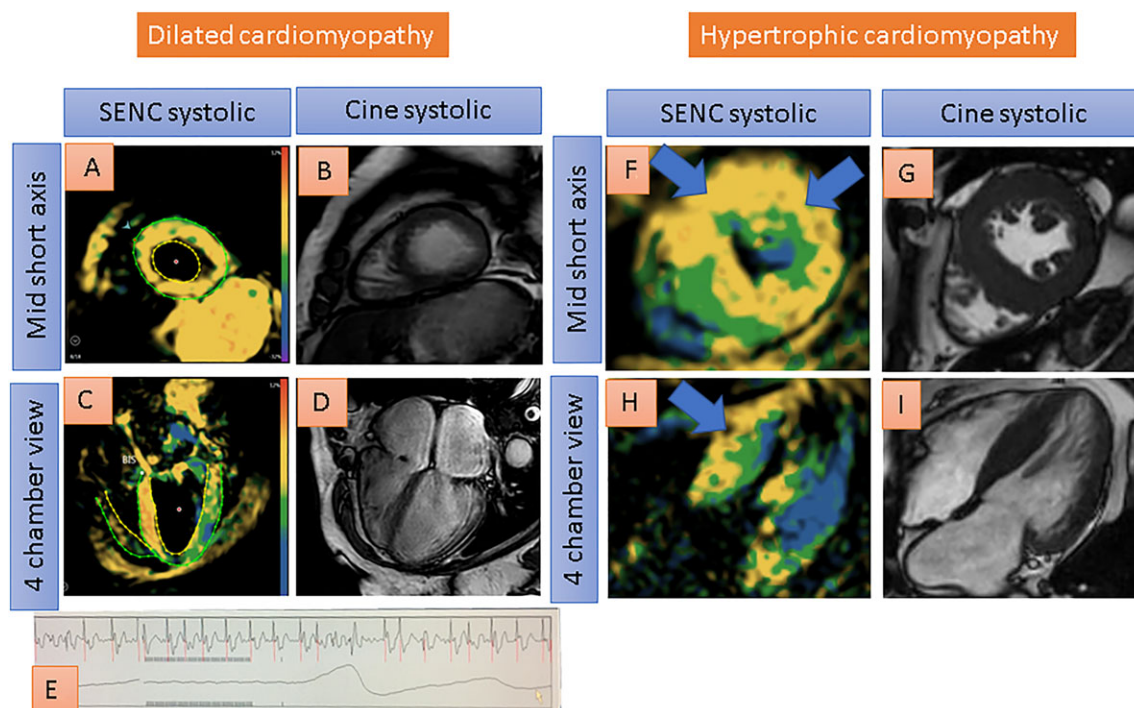
In addition, in Figure 7, reduced myocardial strain is shown by single-heartbeat fast-SENC images (A and B, and E and F) in a patient with cardiac amyloidosis, moderate myocardial hypertrophy, and impaired ejection fraction of ~38% by cine images (C and G). Diffuse LGE can be depicted in D and H.

Table 4 Summary of the studies investigating the ability of SENC to assess myocardial strain in patients with non-ischaemic cardiomyopathies

First author, journal, and year of publication	Disease	Number of patients	Healthy subjects	Quantitative analysis	Comparison with tagged MR	Comparison with LGE
Korosoglou <i>et al.</i> , <i>JMRI</i> , 2008	Non-ischaemic cardiomyopathy	4	Yes <i>n</i> = 12	Yes	Yes	No
Sakamoto <i>et al.</i> , <i>Jpn J Radiol.</i> , 2008	Hypertrophic cardiomyopathy	22	Yes <i>n</i> = 24	Yes	No	Yes
Nakano <i>et al.</i> , <i>Can J Cardiol.</i> , 2013	Cardiac sarcoidosis	1	No	Yes	No	Yes

LGE, late gadolinium enhancement; MR, magnetic resonance.

Figure 6 Single-heartbeat fast-SENC acquisitions of a patient with dilated cardiomyopathy (A–E) and another patient with hypertrophic cardiomyopathy (F–I). Despite atrial fibrillation, good image quality is provided, depicting globally reduced strain using fast-SENC in A and C (reduced strain coded green or yellow by fast-SENC acquisitions). Ejection fraction is ~20% with cine images in B and D. The electrocardiogram shows atrial fibrillation (E). Severe left ventricular hypertrophy, on the other hand, can be appreciated with fast-SENC (F and H) and with systolic cine images (G and I) in another patient with hypertrophic cardiomyopathy. Reduced strain especially in the septum and in the anterior wall (coded yellow) can be depicted with fast-SENC acquisitions (blue arrows in F and H).



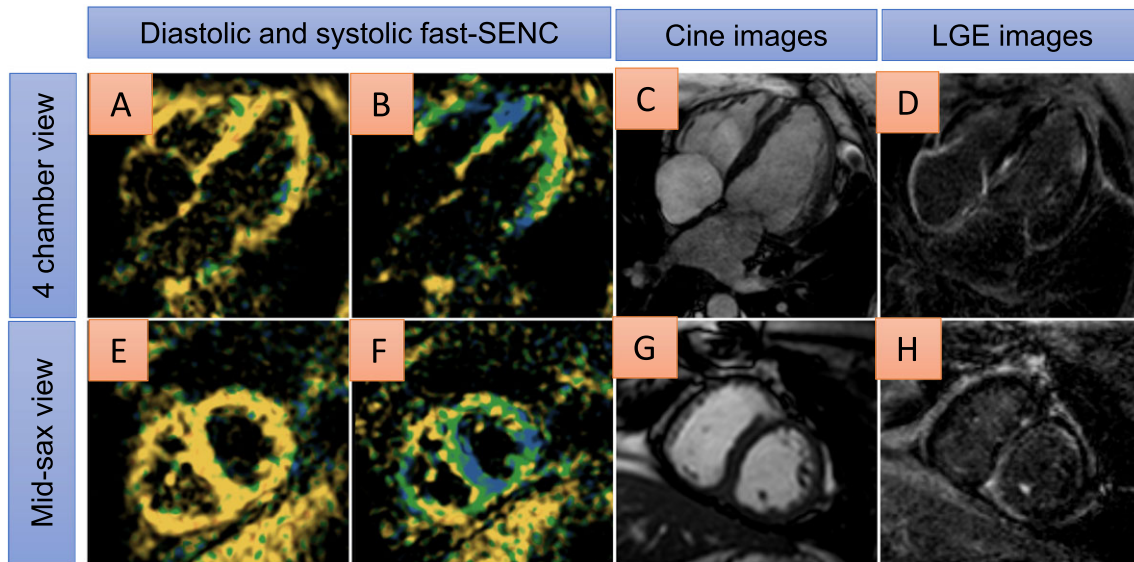
Diabetic heart disease

The prevalence of heart failure is high in patients with diabetes, ranging from 19% to 45%, irrespectively of the presence of CAD and arterial hypertension.^{61,62} A high proportion of such patients with diabetes exhibit diastolic dysfunction with preserved ejection fraction^{63–66} before they present with symptoms of heart failure.⁶⁷ For this reason, the early diagnosis of subtle myocardial dysfunction is crucial in such patients.

The underlying pathophysiologic mechanisms of diabetic heart disease in the absence of significant coronary atherosclerosis are not fully understood. In this regard, it remains

unclear whether diastolic dysfunction is an intrinsic metabolic myocardial disorder with diabetes or whether it is related to impaired microvascular integrity or myocardial fibrosis. A previous study addressed this question using SENC and demonstrated that impaired diastolic function measured as diminished diastolic strain rate is associated with increased triglyceride content in patients with type 2 diabetes mellitus.⁶⁸ All 42 patients included in this study had preserved ejection fraction of >55% and absence of inducible myocardial ischaemia by adenosine stress CMR. These findings agree with those of previous studies, showing that impaired myocardial relaxation is associated with cardiac

Figure 7 Areas of reduced myocardial strain are shown by single-heartbeat fast-SENC images (coded green or yellow in A and B, and E and F) in a patient with cardiac amyloidosis, moderate myocardial hypertrophy, and impaired ejection fraction of ~38% by cine imaging (C and G). Diffuse late gadolinium enhancement (LGE) can be depicted in D and H.



steatosis,^{69,70} which represents an early sign of diabetic heart disease. This is reasonable from a pathophysiologic point of view, due to direct metabolic effects of diabetes mellitus and insulin resistance, causing myocardial dysfunction irrespective of macrovascular or microvascular disease. This hypothesis is also in agreement with a study conducted in women with subclinical heart failure and with preserved ejection fraction (HFpEF), which highlighted an association between triglyceride content and diastolic strain rate by tagged MR.⁷¹ Along the same line, older subjects with an increased prevalence of cardiovascular risk factors, such as diabetes mellitus, exhibited decreased diastolic strain rate by SENC, which was paralleled by increasing myocardial T_1 values, as a surrogate marker of myocardial fibrosis.⁷²

In *Figure 8*, reduced myocardial strain can be depicted by single-heartbeat fast-SENC images especially in the anterior and septal wall (blue arrows in B and F) in a patient with hypertensive and diabetic heart disease and without clinical signs of heart failure. Four-chamber view and short axis cine images (C and D, and G and H) show preserved ejection fraction of 58% in the presence of LV hypertrophy.

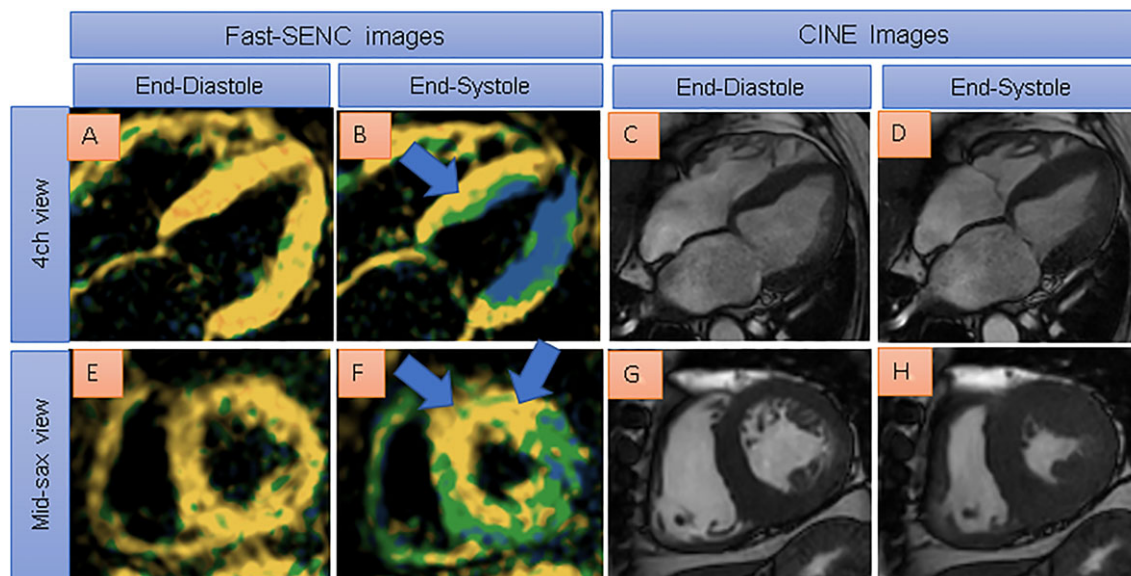
Myocardial strain of the right ventricle in healthy subjects and pulmonary hypertension patients

The right ventricle is a thin-walled cavity, which physiologically acts as a flow generator accommodating the entire venous blood return into the heart. Due to the complex

anatomy of the RV, the tomographic nature of CMR makes it an ideal tool for assessing RV dimensions and function. Indeed, CMR studies have demonstrated high reproducibility for the assessment of RV function in healthy volunteers and in patients with Fallot tetralogy or pulmonary hypertension (PH).⁷³ Assessing the RV anatomy and function is essential, as its role is nowadays widely recognized in heart failure, RV infarction, congenital heart disease, and PH.

Because of the thin wall of the RV, which varies between 2 and 5 mm in healthy subjects,⁷⁴ the assessment of myocardial strain appears particularly challenging. Despite these challenges, SENC depicted increasing circumferential strain from the base to the apex of the RV free wall and demonstrated excellent inter-observer and intra-observer variabilities in 21 healthy subjects who underwent 3.0 T CMR and in another 11 volunteers who underwent single-heartbeat fast-SENC acquisitions.¹⁸ Similar results were acquired in 12 healthy subjects examined in a 3.0 T scanner.⁷⁵ Several subsequent studies investigated regional strain of the RV in patients with PH. Longitudinal and circumferential RV strain was reduced in patients with PH compared with healthy subjects.¹⁹ Taking this one step further, an association between reduced longitudinal strain at the anterior insertion of the RV with local fibrosis in the RV insertion points was demonstrated.⁷⁶ This suggests that in PH, increased afterload may progressively cause mechanical stress at the RV septal insertion points, resulting in local fibrosis and reduced regional longitudinal contraction in the long term. Studying another 37 patients with PH, the midventricular level of the RV was identified as the most sensitive site for the early detection of RV dysfunction in such patients.⁷⁷ In agreement to

Figure 8 Reduced myocardial strain can be depicted by single-heartbeat fast-SENC acquisitions especially in the anterior and septal wall (blue arrows in B and F, severely reduced myocardial strain coded yellow) in a patient with hypertensive and diabetic heart disease. Four chamber view and short axis cine images (C and D, and G and H) show preserved ejection fraction of 58% in the presence of evident left ventricular hypertrophy.



previous data,⁷⁸ longitudinal strain exhibited higher accuracy than circumferential strain for the detection of RV dysfunction.⁷⁷ A good correlation was also observed between CMR-derived strain using SENC and 2D derived RV strain using echocardiographic speckle tracking with CMR-derived RV ejection fraction in 30 consecutive patients with PH.⁷⁹ The correlations between SENC and feature tracking imaging (FTI), on the other hand, exhibited rather moderate correlations in 30 patients with PH and 15 normal subjects. Interestingly, in contrast to FTI, SENC-derived longitudinal strain was significantly lower in patients with PH than in healthy subjects,⁸⁰ indicating the lower accuracy of FTI for the assessment of regional myocardial strain in the RV.

An overview of studies investigating myocardial strain of the right ventricle by SENC in healthy subjects and in patients with PH is provided in *Table 5*.

Early detection of cardiotoxicity

Although previous echocardiographic and CMR studies using tagged MR and Harmonic phase (HARP) have demonstrated the ability of strain imaging to detect preclinical myocardial dysfunction during chemotherapy, studies with SENC are not available in published form so far. Preliminary data, however, support the applicability of SENC in this context, demonstrating high sensitivity for the early detection of cardiotoxicity.

In *Figure 9*, single-heartbeat fast-SENC images of a 57-year-old cardiac asymptomatic patient with B-cell lymphoma and without cardiovascular risk factors can be appreciated. Fast-SENC images prior to chemotherapy exhibit normal myocardial strain in all segments (A and B), and LV ejection fraction was 58%. After 2 cycles of chemotherapy, seven segments show mildly reduced myocardial strain and another two segments show severely reduced myocardial strain (C and D), attributable to cardiac toxicity, although LV ejection fraction remains identical (58%). The patient suffered from fatigue and dyspnoea of New York Heart Association class II.

Comparison between SENC and FTI

Feature tracking imaging is a well-established algorithm for the assessment of myocardial strain. Thus, longitudinal strain assessed by FTI was recently shown to predict clinical outcomes in patients after acute myocardial infarction^{81,82} as well as in patients with chronic ischaemic and non-ischaemic cardiomyopathies.⁸³ Limited data exist however, directly comparing SENC with FTI. Some recent studies, however, have pointed to limitations of the FTI algorithm especially for the assessment of regional function. Thus, in a recent study investigating the observer variability of FTI and tagged MR, the authors found that observer variability with FTI is substantially higher compared with tagging and strongly dependent on the reader's experience.⁸⁴ The low reproducibility of FTI for

Table 5 Summary of the studies investigating the ability of SENC to assess myocardial strain in the right ventricle of normal subjects and patients with pulmonary hypertension (PH)

First author, journal, and year of publication	Number of healthy subjects	Number of patients with PH	Single-heartbeat acquisition	Comparison with LGE	Comparison with 2D echo	Inter-observer variability	Intra-observer variability
Youssef <i>et al.</i> , <i>JMRI</i> , 2008	21	None	No	No	No	$r = 0.80$	$r = 0.88$
Handam <i>et al.</i> , <i>JMRI</i> , 2008	12	None	No	No	No	$r = 0.89^a$	NA
Shehata <i>et al.</i> , <i>MRM</i> , 2010	11	11	Yes	No	No	$0.2\% \pm 5.3\%$	$0.3\% \pm 5.4\%$
Shehata <i>et al.</i> , <i>AJR</i> , 2011	None	32	Yes	Yes	No	NA	NA
Oyama-Manabe <i>et al.</i> , <i>Int. J. Cardiovasc. Imaging</i> , 2013	13	37	Yes	No	No	c	c
Freed <i>et al.</i> , <i>Echocardiography</i> , 2014	None	30	Yes	No	Yes	10%	13%
Ohyama <i>et al.</i> , <i>IJC</i> , 2015	15	30	No	No	No	d	d

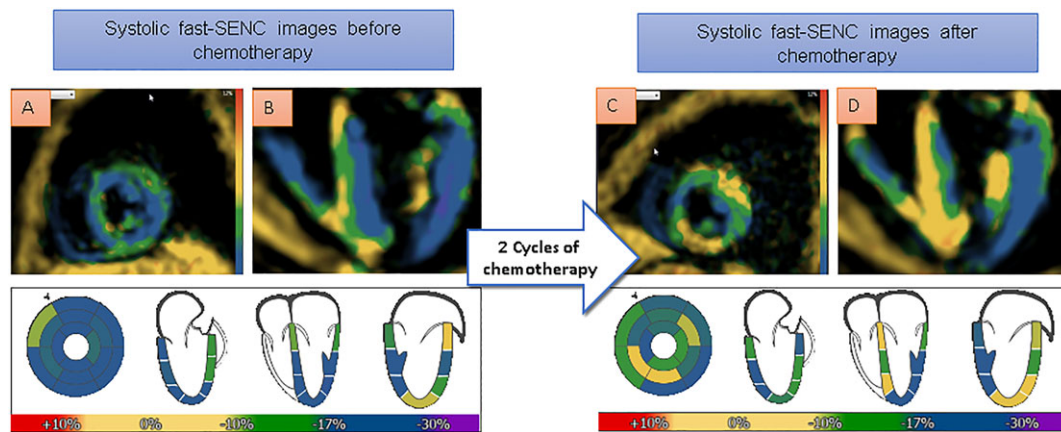
LGE, late gadolinium enhancement; NA, not applicable.

^aFor peak longitudinal strain.

^bFor peak circumferential strain.

^cLow inter-observer and intra-observer variability is demonstrated by Bland–Altman plots. Correlation coefficients are not provided.

^dObserver variability provided only for feature tracking imaging. The discriminatory capacity of SENC was superior to that provided by feature tracking imaging for the detection of right ventricular dysfunction in patients with PH.

Figure 9 Single-heartbeat fast-SENC acquisitions of a 57-year-old cardiac asymptomatic patient with B-cell lymphoma. Fast-SENC images prior to chemotherapy (A and B) exhibit normal myocardial strain (coded blue) in all segments and left ventricular ejection fraction of 58%. After 2 cycles of chemotherapy, seven segments show mildly reduced myocardial strain and another two segments show severely reduced myocardial strain (coded green and yellow, respectively, in C and D), attributable to cardiac toxicity, although left ventricular ejection fraction remains identical (58%).

the assessment of segmental strain was confirmed in a very recent study conducted in 88 healthy adults⁸⁵ and by Almutairi *et al.*, who noticed better reproducibility for global compared with regional strain and referred to the need of validation using physical and numerical phantoms.⁸⁶ In the same direction, baseline strain parameters using FTI CMR 1–3 days after reperfused ST-elevation myocardial infarction were not able to predict adverse LV remodelling,⁸⁷ which is not in agreement with the data reported by Neizel *et al.* for SENC.⁴⁴ Future studies are now warranted to prospectively compare the ability of FTI and SENC for the diagnostic classification and risk stratification of specific myocardial disorders.

Limitations

Our review article has some limitations. Thus, in contrast to FTI, SENC needs a specific image sequence to measure myocardial deformation, whereas limited data exist on a head-to-head comparison between SENC and FTI. In some studies, discussed in this article, e.g. in patients with non-ischaeamic cardiomyopathy, the number of patients included was relatively small, whereas for ischaemia and viability detection, most studies were conducted in the same CMR laboratory, and FFR was not systematically used as the standard reference for assessing the functional significance of CAD. In

addition, T_1 mapping and modern or more sophisticated LGE quantification approaches were not used in these previous studies, whereas SENC was not compared with echocardiographic strain or to FTI in most of these studies. However, with ischaemic heart disease the ability of SENC was not shown only for the diagnostic classification, but more importantly for the prediction of hard cardiac events, such as cardiac death and non-fatal myocardial infarction in such patients. Despite the relatively large amount of scientific evidence, especially with ischaemic heart disease, the SENC sequence is unfortunately to date not yet widely available in CMR centres, which limits its applicability in the clinical routine. In addition, quantification analysis of myocardial strain by SENC has shown higher accuracy for the detection of ischaemia compared with wall motion analysis and higher reproducibility than LV ejection fraction, but such quantification algorithms may be difficult to implement in busy CMR centres. With ischaemia detection, however, the interpretation of colour-coded SENC images during stress can be assessed by visual criteria, promptly leading to the correct diagnosis without the need for quantification analysis. In addition, semiautomatic software developments currently allow the calculation of GLS and GCS with SENC within a relatively short time spent.

Conclusions

Although magnetization saturation techniques enabled quantification assessment of myocardial deformation as early as 1988, it took decades until such techniques became applicable with clinical MR scanners. Since 2001, when SENC was described in the literature,¹ numerous *in vitro* animal and human studies have been performed, demonstrating the abil-

ity of SENC to characterize physiologic heart mechanics and diseases of the heart with high accuracy and reproducibility and without the need for contrast agent administration. Myocardial strain can be assessed visually and quantitatively by SENC, enabling characterization of the heterogeneity of myocardial strain in the human and animal heart and precise diagnostic classification and risk stratification of patients with CAD, myocardial infarction, transplant vasculopathy, non-ischaemic cardiomyopathies, PH, diabetic heart disease, and potentially cardiac toxicity during chemotherapy in cancer patients. In addition, SENC can be applied during pharmacologic CMR stress testing, enabling detection of CAD during intermediate stages of inotropic stimulation, thus shortening the duration of such diagnostic procedures in the interest of time, cost, and patient safety. In this regard, single-heartbeat fast-SENC acquisitions allow the acquisition of myocardial function in free breathing and therefore provide high-quality images even in patients with shortness of breath due to, e.g. heart failure or pulmonary obstruction. Especially in patients with contraindication to gadolinium contrast agents,⁸⁸ SENC represents a valuable alternative for the characterization of underlying myocardial pathologies.

Supporting information

Additional supporting information may be found online in the Supporting Information section at the end of the article.

Figure S1. Supporting information

Table S1. Typical spatial and temporal resolution with cine, tagged MR, SENC and LGE sequences.

Table S2. Providing inter- and intraobserver and interstudy agreement with visual and quantitative SENC studies.

References

- Osman NF, Sampath S, Atalar E, Prince JL. Imaging longitudinal cardiac strain on short-axis images using strain-encoded MRI. *Magn Reson Med* 2001; **46**: 324–334.
- Ibrahim E-SH. Myocardial tagging by cardiovascular magnetic resonance: evolution of techniques–pulse sequences, analysis algorithms, and applications. *J Cardiovasc Magn Reson* 2011; **13**: 36.
- Pan L, Stuber M, Kraitchman DL, Fritzges DL, Gilson WD, Osman NF. Real-time imaging of regional myocardial function using fast-SENC. *Magn Reson Med* 2006; **55**: 386–395.
- Harouni AA, Hossain J, El Khouli R, Matsuda KM, Bluemke DA, Osman NF, Jacobs MA. Strain-encoded breast MRI in phantom and ex vivo specimens with histological validation: preliminary results. *Med Phys* 2012; **39**: 7710–7718.
- Harouni AA, Hossain J, Jacobs MA, Osman NF. Improved hardware for higher spatial resolution strain-encoded (SENC) breast MRI for strain measurements. *Acad Radiol* 2011; **18**: 705–715.
- Harouni AA, Jacobs MA, Osman NF. Finding the optimal compression level for strain-encoded (SENC) breast MRI; simulations and phantom experiments. *Med Image Comput Comput-Assist Interv MICCAI Int Conf Med Image Comput Comput-Assist Interv* 2011; **14**: 444–451.
- Gilson WD, Kraitchman DL. Cardiac magnetic resonance imaging in small rodents using clinical 1.5 T and 3.0 T scanners. *Methods* 2007; **43**: 35–45.
- Ibrahim E-SH, Stuber M, Fahmy AS, Abd-Elmoniem KZ, Sasano T, Abraham MR, Osman NF. Real-time MR imaging of myocardial regional function using strain-encoding (SENC) with tissue through-plane motion tracking. *J Magn Reson Imaging* 2007; **26**: 1461–1470.
- Tanaka A, Kawaji K, Patel AR, Ota T. The extracellular matrix patch implanted in the right ventricle evaluated with cardiovascular magnetic resonance protocol to assess regional biomechanical properties. *Interact Cardiovasc Thorac Surg* 2017; **24**: 82–89.
- Tanaka A, Kawaji K, Patel AR, Tabata Y, Burke MC, Gupta MP, Ota T. In situ

- constructive myocardial remodeling of extracellular matrix patch enhanced with controlled growth factor release. *J Thorac Cardiovasc Surg* 2015; **150**: 1280–1290 e2.
11. Bogaert J, Rademakers FE. Regional nonuniformity of normal adult human left ventricle. *Am J Physiol Heart Circ Physiol* 2001; **280**: H610–H620.
 12. Garot J, Lima JAC, Gerber BL, Sampath S, Wu KC, Bluemke DA, Prince JL, Osman NF. Spatially resolved imaging of myocardial function with strain-encoded MR: comparison with delayed contrast-enhanced MR imaging after myocardial infarction. *Radiology* 2004; **233**: 596–602.
 13. Korosoglou G, Youssef AA, Bilchick KC, Ibrahim E-S, Lardo AC, Lai S, Osman NF. Real-time fast strain-encoded magnetic resonance imaging to evaluate regional myocardial function at 3.0 Tesla: comparison to conventional tagging. *J Magn Reson Imaging* 2008; **27**: 1012–1018.
 14. Lima JA, Jeremy R, Guier W, Bouton S, Zerhouni EA, McVeigh E, Buchalter MB, Weisfeldt ML, Shapiro EP, Weiss JL. Accurate systolic wall thickening by nuclear magnetic resonance imaging with tissue tagging: correlation with sonomicrometers in normal and ischemic myocardium. *J Am Coll Cardiol* 1993; **21**: 1741–1751.
 15. Neizel M, Lossnitzer D, Korosoglou G, Schäufole T, Lewien A, Steen H, Katus HA, Osman NF, Giannitsis E. Strain-encoded (SENC) magnetic resonance imaging to evaluate regional heterogeneity of myocardial strain in healthy volunteers: comparison with conventional tagging. *J Magn Reson Imaging* 2009; **29**: 99–105.
 16. Taqueti VR, Solomon SD, Shah AM, Desai AS, Groarke JD, Osborne MT, Hainer J, Bibbo CF, Dorbala S, Blankstein R, di Carli MF. Coronary microvascular dysfunction and future risk of heart failure with preserved ejection fraction. *Eur Heart J* 2018; **39**: 840–849.
 17. Hamdan A, Thouet T, Kelle S, Wellnhofer E, Paetsch I, Gebker R, Schnackenburg B, Fahmy AS, Osman NF, Bornstedt A, Fleck E. Strain-encoded MRI to evaluate normal left ventricular function and timing of contraction at 3.0 Tesla. *J Magn Reson Imaging* 2009; **29**: 799–808.
 18. Youssef A, Ibrahim E-SH, Korosoglou G, Abraham MR, Weiss RG, Osman NF. Strain-encoding cardiovascular magnetic resonance for assessment of right-ventricular regional function. *J Cardiovasc Magn Reson* 2008; **10**: 33–43.
 19. Shehata ML, Basha TA, Tantawy WH, Lima JA, Vogel-Claussen J, Bluemke DA, Hassoun PM, Osman NF. Real time single heart beat fast strain-encoded imaging of right ventricular regional function: normal versus chronic pulmonary hypertension. *Magn Reson Med* 2010; **64**: 98–106.
 20. Korosoglou G, Gitsioudis G, Voss A, Lehrke S, Riedle N, Buss SJ, Zugck C, Giannitsis E, Osman NF, Katus HA. Strain-encoded cardiac magnetic resonance during high-dose dobutamine stress testing for the estimation of cardiac outcomes: comparison to clinical parameters and conventional wall motion readings. *J Am Coll Cardiol* 2011; **58**: 1140–1149.
 21. Korosoglou G, Lehrke S, Wochele A, Hoerig B, Lossnitzer D, Steen H, Giannitsis E, Osman NF, Katus HA. Strain-encoded CMR for the detection of inducible ischemia during intermediate stress. *JACC Cardiovasc Imaging* 2010; **3**: 361–371.
 22. Nandalur KR, Dwamena BA, Choudhri AF, Nandalur MR, Carlos RC. Diagnostic performance of stress cardiac magnetic resonance imaging in the detection of coronary artery disease: a meta-analysis. *J Am Coll Cardiol* 2007; **50**: 1343–1353.
 23. Lipinski MJ, McVey CM, Berger JS, Kramer CM, Salerno M. Prognostic value of stress cardiac magnetic resonance imaging in patients with known or suspected coronary artery disease: a systematic review and meta-analysis. *J Am Coll Cardiol* 2013; **62**: 826–838.
 24. Bruder O, Wagner A, Lombardi M, Schwitter J, van Rossum A, Pilz G, Nothnagel D, Steen H, Petersen S, Nagel E, Prasad S. European cardiovascular magnetic resonance (EuroCMR) registry—multi national results from 57 centers in 15 countries. *J Cardiovasc Magn Reson* 2013; **15**: 1–9.
 25. Moschetti K, Petersen SE, Pilz G, Kwong RY, Wasserfallen J-B, Lombardi M, Korosoglou G, Van Rossum AC, Bruder O, Mahrholdt H, Schwitter J. Cost-minimization analysis of three decision strategies for cardiac revascularization: results of the “suspected CAD” cohort of the European cardiovascular magnetic resonance registry. *J Cardiovasc Magn Reson* 2016; **18**: 3–13.
 26. Reant P, Labrousse L, Lafitte S, Bordachar P, Pillois X, Tariosse L, Bonoron-Adele S, Padois P, Deville C, Roudaut R, Dos Santos P. Experimental validation of circumferential, longitudinal, and radial 2-dimensional strain during dobutamine stress echocardiography in ischemic conditions. *J Am Coll Cardiol* 2008; **51**: 149–157.
 27. Chan J, Hanekom L, Wong C, Leano R, Cho G-Y, Marwick TH. Differentiation of subendocardial and transmural infarction using two-dimensional strain rate imaging to assess short-axis and long-axis myocardial function. *J Am Coll Cardiol* 2006; **48**: 2026–2033.
 28. Tanaka H, Oishi Y, Mizuguchi Y, Emi S, Ishimoto T, Nagase N, Tabata T, Yamada H, Oki T. Three-dimensional evaluation of dobutamine-induced changes in regional myocardial deformation in ischemic myocardium using ultrasonic strain measurements: the role of circumferential myocardial shortening. *J Am Soc Echocardiogr* 2007; **20**: 1294–1299.
 29. Winter R, Jussila R, Nowak J, Brodin L-A. Speckle tracking echocardiography is a sensitive tool for the detection of myocardial ischemia: a pilot study from the catheterization laboratory during percutaneous coronary intervention. *J Am Soc Echocardiogr* 2007; **20**: 974–981.
 30. Korosoglou G, Lossnitzer D, Schellberg D, Lewien A, Wochele A, Schaeufele T, Neizel M, Steen H, Giannitsis E, Katus HA, Osman NF. Strain-encoded cardiac MRI as an adjunct for dobutamine stress testing: incremental value to conventional wall motion analysis. *Circ Cardiovasc Imaging* 2009; **2**: 132–140.
 31. Korosoglou G, Futterer S, Humpert PM, Riedle N, Lossnitzer D, Hoerig B, Steen H, Giannitsis E, Osman NF, Katus HA. Strain-encoded cardiac MR during high-dose dobutamine stress testing: comparison to cine imaging and to myocardial tagging. *J Magn Reson Imaging* 2009; **29**: 1053–1061.
 32. Stojanovic I, Schneider JE, Cooper J. Cost-impact of cardiac magnetic resonance imaging with fast-SENC compared to SPECT in the diagnosis of coronary artery disease in the US. *J Med Econ* 2019; **22**: 430–438.
 33. Reinstadler SJ, Thiele H, Eitel I. Risk stratification by cardiac magnetic resonance imaging after ST-elevation myocardial infarction. *Curr Opin Cardiol* 2015; **30**: 681–689.
 34. Korosoglou G, Elhmidi Y, Steen H, Schellberg D, Riedle N, Ahrens J, Lehrke S, Merten C, Lossnitzer D, Radeleff J, Zugck C, Giannitsis E, Katus HA. Prognostic value of high-dose dobutamine stress magnetic resonance imaging in 1,493 consecutive patients: assessment of myocardial wall motion and perfusion. *J Am Coll Cardiol* 2010; **56**: 1225–1234.
 35. Wellnhofer E, Olariu A, Klein C, Gräfe M, Wahl A, Fleck E, Nagel E. Magnetic resonance low-dose dobutamine test is superior to SCAR quantification for the prediction of functional recovery. *Circulation* 2004; **109**: 2172–2174.
 36. Glaveckaitė S, Valeviciene N, Palionis D, Skorniakov V, Celutkienė J, Tamosiunas A, Uzdavinyš G, Laucevičius A. Value of scar imaging and inotropic reserve combination for the prediction of segmental and global left ventricular functional recovery after revascularisation. *J Cardiovasc Magn Reson* 2011; **13**: 35–47.
 37. Romero J, Xue X, Gonzalez W, Garcia MJ. CMR imaging assessing viability in patients with chronic ventricular dysfunction due to coronary artery disease: a meta-analysis of prospective trials. *JACC Cardiovasc Imaging* 2012; **5**: 494–508.
 38. Hammer-Hansen S, Bandettini WP, Hsu L-Y, Leung SW, Shanbhag S, Mancini C, Greve AM, Køber L, Thune JJ, Kellman P, Arai AE. Mechanisms for

- overestimating acute myocardial infarct size with gadolinium-enhanced cardiovascular magnetic resonance imaging in humans: a quantitative and kinetic study. *Eur Heart J Cardiovasc Imaging* 2016; **17**: 76–84.
39. Kramer CM, Rogers WJ, Theobald TM, Power TP, Petruolo S, Reichek N. Remote noninfarcted region dysfunction soon after first anterior myocardial infarction. A magnetic resonance tagging study. *Circulation* 1996; **94**: 660–666.
40. Koos R, Altiok E, Doetsch J, Neizel M, Krombach G, Marx N, Hoffmann R. Layer-specific strain-encoded MRI for the evaluation of left ventricular function and infarct transmuralty in patients with chronic coronary artery disease. *Int J Cardiol* 2013; **166**: 85–89.
41. Altiok E, Neizel M, Tiemann S, Krass V, Becker M, Zwicker C, Koos R, Kelm M, Kraemer N, Schoth F, Marx N, Hoffmann R. Layer-specific analysis of myocardial deformation for assessment of infarct transmuralty: comparison of strain-encoded cardiovascular magnetic resonance with 2D speckle tracking echocardiography. *Eur Heart J Cardiovasc Imaging* 2013; **14**: 570–578.
42. Oyama-Manabe N, Ishimori N, Sugimori H, Van Cauteren M, Kudo K, Manabe O, Okuaki T, Kamishima T, Ito YM, Tsutsui H, Tha KK. Identification and further differentiation of subendocardial and transmural myocardial infarction by fast strain-encoded (SENC) magnetic resonance imaging at 3.0 Tesla. *Eur Radiol* 2011; **21**: 2362–2368.
43. Neizel M, Lossnitzer D, Korosoglou G, Schäufele T, Peykarjou H, Steen H, Ocklenburg C, Giannitsis E, Katus HA, Osman NF. Strain-encoded MRI for evaluation of left ventricular function and transmuralty in acute myocardial infarction. *Circ Cardiovasc Imaging* 2009; **2**: 116–122.
44. Neizel M, Korosoglou G, Lossnitzer D, Kühl H, Hoffmann R, Ocklenburg C, Giannitsis E, Osman NF, Katus HA, Steen H. Impact of systolic and diastolic deformation indexes assessed by strain-encoded imaging to predict persistent severe myocardial dysfunction in patients after acute myocardial infarction at follow-up. *J Am Coll Cardiol* 2010; **56**: 1056–1062.
45. Taylor DO, Edwards LB, Boucek MM, Trulock EP, Aurora P, Christie J, Dobbels F, Rahmel AO, Keck BM, Hertz MI. Registry of the International Society for Heart and Lung Transplantation: twenty-fourth official adult heart transplant report—2007. *J Heart Lung Transplant* 2007; **26**: 769–781.
46. Kobashigawa JA, Tobis JM, Starling RC, Tuzcu EM, Smith AL, Valentine HA, Yeung AC, Mehra MR, Anzai H, Oeser BT, Abeywickrama KH, Murphy J, Cretin N. Multicenter intravascular ultrasound validation study among heart transplant recipients: outcomes after five years. *J Am Coll Cardiol* 2005; **45**: 1532–1537.
47. Tuzcu EM, Kapadia SR, Sachar R, Ziada KM, Crowe TD, Feng J, Magyar WA, Hobbs RE, Starling RC, Young JB, McCarthy P, Nissen SE. Intravascular ultrasound evidence of angiographically silent progression in coronary atherosclerosis predicts long-term morbidity and mortality after cardiac transplantation. *J Am Coll Cardiol* 2005; **45**: 1538–1542.
48. Topol EJ, Nissen SE. Our preoccupation with coronary luminology. The dissociation between clinical and angiographic findings in ischemic heart disease. *Circulation* 1995; **92**: 2333–2342.
49. Hofmann NP, Steuer C, Voss A, Erbel C, Celik S, Doesch A, Ehlermann P, Giannitsis E, Buss SJ, Katus HA, Korosoglou G. Comprehensive bioimaging using myocardial perfusion reserve index during cardiac magnetic resonance imaging and high-sensitive troponin T for the prediction of outcomes in heart transplant recipients. *Am J Transplant* 2014; **14**: 2607–2616.
50. Steen H, Merten C, Refle S, Klingenberg R, Dengler T, Giannitsis E, Katus HA. Prevalence of different gadolinium enhancement patterns in patients after heart transplantation. *J Am Coll Cardiol* 2008; **52**: 1160–1167.
51. Korosoglou G, Osman NF, Dengler TJ, Riedle N, Steen H, Lehrke S, Giannitsis E, Katus HA. Strain-encoded cardiac magnetic resonance for the evaluation of chronic allograft vasculopathy in transplant recipients. *Am J Transplant* 2009; **9**: 2587–2596.
52. Erbel C, Mukhammadaminova N, Gleissner CA, Osman NF, Hofmann NP, Steuer C, Akhavanpoor M, Wangler S, Celik S, Doesch AO, Voss A, Buss SJ, Schnabel PA, Katus HA, Korosoglou G. Myocardial perfusion reserve and strain-encoded CMR for evaluation of cardiac allograft microvasculopathy. *JACC Cardiovasc Imaging* 2016; **9**: 255–266.
53. Maron BJ, Towbin JA, Thiene G, Antzelevitch C, Corrado D, Arnett D, Moss AJ, Seidman CE, Young JB, American Heart Association, Council on Clinical Cardiology, Heart Failure and Transplantation Committee, Quality of Care and Outcomes Research and Functional Genomics and Translational Biology Interdisciplinary Working Groups, Council on Epidemiology and Prevention. Contemporary definitions and classification of the cardiomyopathies. *Circulation* 2006; **113**: 1807–1816.
54. Pennell D. Cardiovascular magnetic resonance. *Heart* 2001; **85**: 581–589.
55. Assomull RG, Prasad SK, Lyne J, Smith G, Burman ED, Khan M, Sheppard MN, Poole-Wilson PA, Pennell DJ. Cardiovascular magnetic resonance, fibrosis, and prognosis in dilated cardiomyopathy. *J Am Coll Cardiol* 2006; **48**: 1977–1985.
56. Lehrke S, Lossnitzer D, Schöb M, Steen H, Merten C, Kemmling H, Pribe R, Ehlermann P, Zugck C, Korosoglou G, Giannitsis E. Use of cardiovascular magnetic resonance for risk stratification in chronic heart failure: prognostic value of late gadolinium enhancement in patients with non-ischaemic dilated cardiomyopathy. *Heart* 2011; **97**: 727–732.
57. Giusca S, Korosoglou G, Zieschang V, Stoiber L, Schnackenburg B, Stehning C, Gebker R, Pieske B, Schuster A, Backhaus S, Pieske-Kraigher E, Patel A, Kawaji K, Steen H, Lapinskas T, Kelle S. Reproducibility study on myocardial strain assessment using fast-SENC cardiac magnetic resonance imaging. *Sci Rep* 2018; **8**: 14100.
58. Sakamoto K, Oyama-Manabe N, Manabe O, Aikawa T, Kikuchi Y, Sasai-Masuko H, Naya M, Kudo K, Kato F, Tamaki N, Shirato H. Heterogeneity of longitudinal and circumferential contraction in relation to late gadolinium enhancement in hypertrophic cardiomyopathy patients with preserved left ventricular ejection fraction. *Jpn J Radiol* 2018; **36**: 103–112.
59. Orii M, Hirata K, Tanimoto T, Shiono Y, Shimamura K, Yamano T, Ino Y, Yamaguchi T, Kubo T, Tanaka A, Imanishi T, Akasaka T. Myocardial damage detected by two-dimensional speckle-tracking echocardiography in patients with extracardiac sarcoidosis: comparison with magnetic resonance imaging. *J Am Soc Echocardiogr* 2015; **28**: 683–691.
60. Nakano S, Kimura F, Osman N, Sugi K, Tanno J, Uchida Y, Shiono A, Senbonmatsu T, Nishimura S. Improved myocardial strain measured by strain-encoded magnetic resonance imaging in a patient with cardiac sarcoidosis. *Can J Cardiol* 2013; **29**: 1531.e9–11.
61. Thrainsdottir IS, Aspelund T, Thorgeirsson G, Gudnason V, Hardarson T, Malmberg K, Sigurdsson G, Ryden L. The association between glucose abnormalities and heart failure in the population-based Reykjavik study. *Diabetes Care* 2005; **28**: 612–616.
62. Gottdiener JS, Arnold AM, Aurigemma GP, Polak JF, Tracy RP, Kitzman DW, Gardin JM, Rutledge JE, Boineau RC. Predictors of congestive heart failure in the elderly: the Cardiovascular Health Study. *J Am Coll Cardiol* 2000; **35**: 1628–1637.
63. Boyer JK, Thanigaraj S, Schechtman KB, Pérez JE. Prevalence of ventricular diastolic dysfunction in asymptomatic, normotensive patients with diabetes mellitus. *Am J Cardiol* 2004; **93**: 870–875.
64. Redfield MM, Jacobsen SJ, Burnett JC, Mahoney DW, Bailey KR, Rodeheffer RJ. Burden of systolic and diastolic ventricular dysfunction in the community: appreciating the scope of the heart failure epidemic. *JAMA* 2003; **289**: 194–202.
65. Zabalgoitia M, Ismaeil MF, Anderson L, Maklady FA. Prevalence of diastolic dysfunction in normotensive, asymptomatic

- patients with well-controlled type 2 diabetes mellitus. *Am J Cardiol* 2001; **87**: 320–323.
66. de Simone G, Devereux RB, Chinali M, Lee ET, Galloway JM, Barac A, Panza JA, Howard BV. Diabetes and incident heart failure in hypertensive and normotensive participants of the Strong Heart Study. *J Hypertens* 2010; **28**: 353–360.
 67. de Boer RA, Doehner W, van der Horst ICC, Anker SD, Babalis D, Roughton M, Coats AJ, Flather MD, van Veldhuisen DJ, SENIORS Investigators. Influence of diabetes mellitus and hyperglycemia on prognosis in patients ≥ 70 years old with heart failure and effects of nebivolol (data from the Study of Effects of Nebivolol Intervention on Outcomes and Rehospitalization in Seniors with heart failure [SENIORS]). *Am J Cardiol* 2010; **106**: 78–86.e1.
 68. Korosoglou G, Humpert PM, Ahrens J, Oikonomou D, Osman NF, Gitsioudis G, Buss SJ, Steen H, Schnackenburg B, Bierhaus A, Nawroth PP, Katus HA. Left ventricular diastolic function in type 2 diabetes mellitus is associated with myocardial triglyceride content but not with impaired myocardial perfusion reserve. *J Magn Reson Imaging* 2012; **35**: 804–811.
 69. Rijzewijk LJ, van der Meer RW, Smit JWA, Diamant M, Bax JJ, Hammer S, Romijn JA, de Roos A, Lamb HJ. Myocardial steatosis is an independent predictor of diastolic dysfunction in type 2 diabetes mellitus. *J Am Coll Cardiol* 2008; **52**: 1793–1799.
 70. Ng ACT, Delgado V, Bertini M, van der Meer RW, Rijzewijk LJ, Hooi Ewe S, Siebelink HM, Smit JWA, Diamant M, Romijn JA, de Roos A, Leung DY, Lamb HJ, Bax JJ. Myocardial steatosis and biventricular strain and strain rate imaging in patients with type 2 diabetes mellitus. *Circulation* 2010; **122**: 2538–2544.
 71. Wei J, Nelson MD, Szczepaniak EW, Smith L, Mehta PK, Thomson LEJ, Berman DS, Li D, Bairey Merz CN, Szczepaniak LS. Myocardial steatosis as a possible mechanistic link between diastolic dysfunction and coronary microvascular dysfunction in women. *Am J Physiol Heart Circ Physiol* 2016; **310**: H14–H19.
 72. Bönner F, Janzarik N, Jacoby C, Spieker M, Schnackenburg B, Range F, Butzbach B, Haberkorn S, Westenfeld R, Neizel-Wittke M, Flögel U. Myocardial T2 mapping reveals age- and sex-related differences in volunteers. *J Cardiovasc Magn Reson* 2015; **17**: 9–21.
 73. American College of Cardiology Foundation Task Force on Expert Consensus Documents, Hundley WG, Bluemke DA, Finn JP, Flamm SD, Fogel MA, Friedrich MG, Ho VB, Jerosch-Herold M, Kramer CM, Manning WJ, Patel M. ACCF/ACR/AHA/NASCI/SCMR 2010 expert consensus document on cardiovascular magnetic resonance: a report of the American College of Cardiology Foundation Task Force on Expert Consensus Documents. *Circulation* 2010; **121**: 2462–2508.
 74. Haddad F, Hunt SA, Rosenthal DN, Murphy DJ. Right ventricular function in cardiovascular disease, part I: anatomy, physiology, aging, and functional assessment of the right ventricle. *Circulation* 2008; **117**(1524–4539 (Electronic)): 1436–1448.
 75. Hamdan A, Thouet T, Kelle S, Paetsch I, Gebker R, Wellnhofer E, Schnackenburg B, Fahmy AS, Osman NF, Fleck E. Regional right ventricular function and timing of contraction in healthy volunteers evaluated by strain-encoded MRI. *J Magn Reson* 2008; **28**: 1379–1385.
 76. Shehata ML, Lossnitzer D, Skrok J, Boyce D, Lechtzin N, Mathai SC, Girgis RE, Osman N, Lima JAC, Bluemke DA, Hassoun PM, Vogel-Claussen J. Myocardial delayed enhancement in pulmonary hypertension: pulmonary hemodynamics, right ventricular function, and remodeling. *AJR Am J Roentgenol* 2011; **196**: 87–94.
 77. Oyama-Manabe N, Sato T, Tsujino I, Kudo K, Manabe O, Kato F, Osman NF, Terae S. The strain-encoded (SENC) MR imaging for detection of global right ventricular dysfunction in pulmonary hypertension. *Int J Cardiovasc Imaging* 2013; **29**: 371–378.
 78. Gilson WD, Yang Z, French BA, Epstein FH. Measurement of myocardial mechanics in mice before and after infarction using multislice displacement-encoded MRI with 3D motion encoding. *Am J Physiol Heart Circ Physiol* 2005; **288**: H1491–H1497.
 79. Freed BH, Tsang W, Bhavne NM, Patel AR, Weinert L, Yamat M, Vicedo BM, Dill K, Mor-Avi V, Gomberg-Maitland M, Lang RM. Right ventricular strain in pulmonary arterial hypertension: a 2D echocardiography and cardiac magnetic resonance study. *Echocardiography* 2015; **32**: 257–263.
 80. Ohyama Y, Ambale-Venkatesh B, Chamara E, Shehata ML, Corona-Villalobos CP, Zimmerman SL, Hassoun PM, Bluemke DA, Lima JAC. Comparison of strain measurement from multimodality tissue tracking with strain-encoding MRI and harmonic phase MRI in pulmonary hypertension. *Int J Cardiol* 2015; **182**: 342–348.
 81. Eitel I, Stiermaier T, Lange T, Rommel K-P, Koschalka A, Kowallick JT, Lotz J, Kutty S, Gutberlet M, Hasenfuß G, Thiele H, Schuster A. Cardiac magnetic resonance myocardial feature tracking for optimized prediction of cardiovascular events following myocardial infarction. *JACC Cardiovasc Imaging* 2018; **11**: 1433–1444.
 82. Gavara J, Rodriguez-Palomares JF, Valente F, Monmeneu JV, Lopez-Lereu MP, Bonanad C, Ferreira-Gonzalez I, Garcia del Blanco B, Rodriguez-Garcia J, Mutuberria M, de Dios E, Rios-Navarro C, Perez-Sole N, Racugno P, Paya A, Minana G, Canoves J, Pellicer M, Lopez-Fornas FJ, Barrabes J, Evangelista A, Nunez J, Chorro FJ, Garcia-Dorado D, Bodi V. Prognostic value of strain by tissue tracking cardiac magnetic resonance after ST-segment elevation myocardial infarction. *JACC Cardiovasc Imaging* 2018; **11**: 1448–1457.
 83. Romano S, Judd RM, Kim RJ, Kim HW, Klem I, Heitner JF, Shah DJ, Jue J, White BE, Indorkar R, Shenoy C, Farzaneh-Far A. Feature-tracking global longitudinal strain predicts death in a multicenter population of patients with ischemic and nonischemic dilated cardiomyopathy incremental to ejection fraction and late gadolinium enhancement. *JACC Cardiovasc Imaging* 2018; **11**: 1419–1429.
 84. Feisst A, Kuetting DLR, Dabir D, Luetkens J, Homsy R, Schild HH, Thomas D. Influence of observer experience on cardiac magnetic resonance strain measurements using feature tracking and conventional tagging. *IJC Heart Vasc* 2018; **18**: 46–51.
 85. Mangion K, Burke NMM, McComb C, Carrick D, Woodward R, Berry C. Feature-tracking myocardial strain in healthy adults—a magnetic resonance study at 3.0 tesla. *Sci Rep* 2019; **9**: 3239–3248.
 86. Almutairi HM, Boubertakh R, Miquel ME, Petersen SE. Myocardial deformation assessment using cardiovascular magnetic resonance-feature tracking technique. *Br J Radiol* 2017; **90**: 20170072.
 87. Shetye AM, Nazir SA, Razvi NA, Price N, Khan JN, Lai FY, Squire IB, McCann GP, Arnold JR. Comparison of global myocardial strain assessed by cardiovascular magnetic resonance tagging and feature tracking to infarct size at predicting remodelling following STEMI. *BMC Cardiovasc Disord* 2017; **17**: 7–14.
 88. Khawaja AZ, Cassidy DB, Al Shakarchi J, McGrogan DG, Inston NG, Jones RG. Revisiting the risks of MRI with Gadolinium based contrast agents—review of literature and guidelines. *Insights Imaging* 2015; **6**: 553–558.